

## THE PROPER MOTION OF THE MAGELLANIC CLOUDS. II. NEW RESULTS FOR FIVE SMALL MAGELLANIC CLOUD FIELDS

EDGARDO COSTA<sup>1</sup>, RENÉ A. MÉNDEZ<sup>1</sup>, MARIO H. PEDREROS<sup>2</sup>, MAXIMILIANO MOYANO<sup>1</sup>, CARME GALLART<sup>3</sup>, AND NOELIA NOËL<sup>4</sup>

<sup>1</sup>Departamento de Astronomía, Universidad de Chile, Casilla 36-D, Santiago, Chile; [costa@das.uchile.cl](mailto:costa@das.uchile.cl), [rmendez@das.uchile.cl](mailto:rmendez@das.uchile.cl), [mmoyano@das.uchile.cl](mailto:mmoyano@das.uchile.cl), [mmoyano@mpia-hd.mpg.de](mailto:mmoyano@mpia-hd.mpg.de)

<sup>2</sup>Departamento de Física, Universidad de Tarapacá, Casilla 7-D, Arica, Chile; [mpedrero@uta.cl](mailto:mpedrero@uta.cl)

<sup>3</sup>Instituto de Astrofísica de Canarias, Tenerife 38200, Islas Canarias, Spain; [carme@iac.es](mailto:carme@iac.es)

<sup>4</sup>Max-Planck-Institut für Astronomie, Königstuhl 17, 69117 Heidelberg, Germany; [noelia@mpia-hd.mpg.de](mailto:noelia@mpia-hd.mpg.de)

Received 2010 October 18; accepted 2011 January 31; published 2011 March 11

### ABSTRACT

We present new results from a ground-based program to determine the proper motion of the Magellanic Clouds (MCs) relative to background quasars (QSOs), being carried out with the Iréneé du Pont 2.5 m telescope at Las Campanas Observatory, Chile. The data were secured over a time base of seven years and with eight epochs of observation. “As measured” (field) proper motions were obtained for five QSO fields in the Small Magellanic Cloud (SMC): QJ0033–7028, QJ0035–7201, QJ0047–7530, QJ0102–7546, and QJ0111–7249. Assuming that the SMC has a disklike central structure, but that it does not rotate, we determined a center-of-mass (CM) proper motion for the SMC from two of these fields, QJ0033–7028 and QJ0035–7201, located to the northwest and west of the main body of the SMC, respectively. Combining these latter proper motions with the CM proper motion presented by Costa et al. (hereafter CMP09) for the SMC (from the field QJ0036–7227, located to the west of the main body of the SMC), we obtain a weighted mean of  $\mu_\alpha \cos \delta = +0.93 \pm 0.14 \text{ mas yr}^{-1}$  and  $\mu_\delta = -1.25 \pm 0.11 \text{ mas yr}^{-1}$ . This CM proper motion is in good agreement with recent results by Piatek et al. and Vieira et al., and we are confident that it is a good representation of the “bulk” transverse motion of the SMC. On the contrary, the results we obtain from the fields QJ0047–7530 and QJ0102–7546, located to the south of the main body of the SMC, and the field QJ0111–7249, located to the east of its main body, *seem* to be affected by streaming motions. For this reason, we have not used the latter to determine the SMC CM proper motion. These streaming motions could be evidence that the SMC was tidally disrupted in a close encounter with the Large Magellanic Cloud (LMC). Complementing the SMC CM proper motions given here and in CMP09, with the currently accepted radial velocity of its center, we have derived its galactocentric (gc) velocity components, obtaining a weighted mean of  $V_{\text{gc,t}} = +289 \pm 25 \text{ km s}^{-1}$  and  $V_{\text{gc,r}} = +14 \pm 24 \text{ km s}^{-1}$ . These velocities, together with the galactocentric velocity components given for the LMC in CMP09, imply a relative velocity between the LMC and SMC of  $67 \pm 42 \text{ km s}^{-1}$  for  $V_{\text{rot,LMC}} = 50 \text{ km s}^{-1}$  and of  $98 \pm 48 \text{ km s}^{-1}$  for  $V_{\text{rot,LMC}} = 120 \text{ km s}^{-1}$ . Despite our large errors, these values are consistent with the standard assumption that the MCs are gravitationally bound to each other.

**Key words:** astrometry – Local Group – Magellanic Clouds

*Online-only material:* color figures

### 1. INTRODUCTION

This is the second of a series of papers devoted to the study of the absolute proper motion of the Magellanic Clouds (MCs). A detailed description of the scientific motivations that prompted the present survey, including a brief history about this and other observational programs to determine their proper motion, can be found in Costa et al. (2009, hereafter CMP09). There we also summarize some theoretical efforts to model the Milky Way (MW)–MCs system, looking for Magellanic orbits that best reproduce conspicuous features, such as the Magellanic Stream (MS), which are believed to be the result of dynamical interactions of this triple system and establish if the MCs are gravitationally bound to each other and if they are bound to the MW.

To elucidate these matters, (1) additional physics is needed to more quantitatively model the observed properties of the MS and other features of the Magellanic system and (2) it is necessary to improve the precision of the space velocity vectors of the MCs to better constrain the models. Considering that their radial velocities are well established, this latter requirement currently resumes the task of precisely measuring their proper motions in order to determine their transverse velocities. Measuring the

proper motions of the MCs is the main motivation of the present research.

Here, we present new results from a ground-based program to determine the proper motion of the MCs relative to background quasars (QSOs), being carried out with the Iréneé du Pont 2.5 m telescope (C100) at Las Campanas Observatory, Chile. The data were secured over a time base of seven years and with eight epochs of observation. In CMP09, we presented center-of-mass (CM) proper motions for the Large Magellanic Cloud (LMC) and Small Magellanic Cloud (SMC), based on two QSO fields, Q0557–6713 of the LMC and Q0036–7227 of the SMC, and in this paper we give “as measured” (field) proper motions for five QSO fields of the SMC: QJ0033–7028, QJ0035–7201, QJ0047–7530, QJ0102–7546, and QJ0111–7249. From two of these (QJ0033–7028 and QJ0035–7201), we derived a CM proper motion for the SMC. In Table 1, we give positional information about the five SMC QSO fields reported in this paper, and in Table 2 we summarize the observational material acquired for them. Their spatial location is illustrated in Figure 2 of CMP09.

Our astrometry program is part of a more comprehensive study of the SMC–LMC–MW system, which includes determining the star formation history of the MCs via comparison of

**Table 1**  
SMC Quasar Fields Reported

QSO	R.A. (J2000.0)	Decl. (J2000.0)	Galaxy
QJ0033–7028	00 33 55.7	–70 29 00	SMC
QJ0035–7201	00 35 29.7	–72 01 23	SMC
QJ0047–7530	00 47 40.8	–75 30 10	SMC
QJ0102–7546	01 02 18.3	–75 46 49	SMC
QJ0111–7249	01 11 41.7	–72 49 47	SMC

**Table 2**  
Observational Material

SMC Field	Epochs	Astrometry Frames	Epoch Range	DCR Frames
QJ0033–7028	8	57	2001.79–2008.83	16
QJ0035–7201	8	51	2001.79–2008.84	15
QJ0047–7530	8	42	2001.79–2008.83	17
QJ0102–7546	8	59	2001.80–2008.84	19
QJ0111–7249	8	59	2001.80–2008.84	19

color–magnitude diagrams (CMDs) of MC fields with synthetic CMDs (see Noël et al. 2007, 2009). This study should lead to a greater understanding of the evolution of the Magellanic system and provide insight into the role of the interactions between the MCs and the MW in stimulating star formation in the MCs and on the formation of the Galactic halo.

## 2. OBSERVATIONS AND CALIBRATIONS

Only a brief description is given here. Full details can be found in CMP09.

The observations were made with a Tektronic 2048 × 2048 pixel<sup>2</sup> CCD detector, with 24 μm pixels, attached to the Cassegrain focus of the C100 telescope at Las Campanas Observatory. This setup provides direct imaging over a field of ∼8′.85 × 8′.85, with a scale of ∼0′.26 pixel<sup>−1</sup>.

Between six and nine astrometric frames were obtained, per epoch, for each QSO field. To minimize the effects of refraction, all astrometric observations were carried out in the *R* bandpass and restricted to hour angles less than ∼1.5 hr. Although in these conditions refraction effects are minor, to model the effect of Differential Color Refraction (DCR) on the measured positions, “DCR Series” (see Section 3.4 and Table 2) were also obtained for each field.

All *R* bandpass frames were exposed for 600 s and were secured in dark time and under seeing conditions that varied between 0′.7 and 1′.3. This yielded a signal-to-noise ratio (S/N) of ∼150 over the full point-spread function (PSF) for the faintest objects of interest (*R* ∼ 20.5).

To reduce the effect of optical distortions on the relative position of the QSO and the local system of reference stars used to determine the proper motion, and also ensuring that all reference stars are present in all images of a given QSO field, each QSO was placed in all corresponding frames within a few pixels of a certain position (selected on the first epoch of observations).

The CCD frames were calibrated using standard IRAF<sup>5</sup> (version 2.11.3) tasks. For this purpose, Zero frames and Dome Flat frames were taken every night.

## 3. THE ASTROMETRY

To determine the proper motion of the SMC, we have used the QSO method. In this method, the position at different epochs of QSOs present in the background of the SMC is measured with respect to bona fide SMC stars. Because QSOs can be considered fiducial points, any motion detected for them will be a reflection of the motion of the local field of SMC stars. A full description of the astrometric procedure can be found in CMP09 and in Méndez et al. (2010).

In this latter paper, on the proper motion of Fornax, we explain in detail various sanity tests that were applied to our SMC data (and, obviously, to our Fornax data), but were briefly (or not) described in CMP09. They can be summarized as experiments to (1) test the effect in the precision of the final pixel coordinates of the various PSF-fitting parameters and detect possible (related) trends with position, brightness, and color of the reference stars; (2) select the relevant terms and order of the polynomial used in the registration process (aimed at minimizing the rms of the transformation and removing trends in the registration residuals); and (3) test the sensitivity of our proper motions to the number of reference stars and detect possible trends due to their brightness and color.

### 3.1. Pixel Coordinates

The coordinates of the background QSOs and field stars on each CCD frame were determined using the various routines within the DAOPHOT package (Stetson 1987).

All frames available for each QSO field were first examined to identify, on the basis of image quality, the best of them (the “Master” frame) and also the best set of consecutive frames. This latter set is used to establish a reference system with respect to which the motion of the QSO is measured: the “Standard Frame of Reference” (SFR), and the Master frame is used to make a preliminary selection of the field stars that will define the SFR. All of the above frames turned out to have stellar images with an average FWHM of ∼0′.7.

With this procedure roughly 300 (depending on the stellar density of each field) isolated, well-exposed (S/N better than ∼150), and homogeneously distributed stars were selected in each field. This set of stars defines the *initial* local reference system common to all frames of a given QSO field. Additional cleansing, to ensure that each local reference system is composed only of SMC stars, is done at a later stage (see Section 3.6).

A subset of typically 180 of the stars defining the initial local reference system in each QSO field was selected to determine a Master PSF for each frame available for that field. For this purpose, we used the task PSF with *function* = *auto* and *varoder* = 2, thus allowing the PSF to vary with position on the CCD chip. Finally, and by means of the task PEAK, the Master PSFs were used to calculate the (*X*, *Y*) centroids of the QSO and reference stars. The identification numbers given in our tables and figures are ID numbers from the PEAK task outputs.

### 3.2. Barycentric Coordinates

Because of their greater stability, which allows for a much better positional precision at this stage of our procedure (i.e., before final registration), all calculations starting at this point were carried out in barycentric coordinates. These coordinates are defined as  $X_i - \bar{X}$ ,  $Y_i - \bar{Y}$ , where  $(\bar{X}, \bar{Y})$  (the “barycenter”) is the average of the (*X*, *Y*) coordinates of the reference stars. This

<sup>5</sup> IRAF is distributed by the National Optical Astronomy Observatory, which is operated by the Association of Universities for Research in Astronomy, Inc., under cooperative agreement with the National Science Foundation.

procedure reduces the negative impact of small offsets between frames, poor guiding, etc.

### 3.3. Differential Color Refraction Correction

For very precise relative astrometry, DCR requires a special treatment. Because atmospheric refraction is wavelength-dependent, stars of different spectral energy distribution (SED) suffer different amounts of refraction. In our case, given that the SED of the background QSOs is different from that of a typical SMC field star, this effect can be particularly important and could induce a systematic shift of the QSO's coordinates with respect to the reference stars. The CMDs of the stars used to define the *final* local reference in QSO fields reported here and in CMP09 (Figures 11–15 here and Figures 16 and 17 in CMP09) show that we are measuring a rather “bluish” object (the QSO) relative to a system composed mainly of SMC red giants.

To model the effect of DCR on the measured positions, one DCR series (a set of about 20 *sequential* images of each QSO field, with hour angles spanning from  $\sim 0.5$  to  $\sim 3.5$  hr from the meridian) was obtained for each QSO field. These observations allowed us to determine the shift due to DCR of the barycentric coordinates of the QSOs and reference stars as a function of hour angle. Example DCR series plots are shown in Figures 3 and 4 of CMP09.

After removing the effects of DCR from the data, it is possible to include relatively large hour angle frames in the proper motion determination. Using the error in the final proper motion of the background QSO as an indicator, an iterative process was adopted to decide the maximum hour angle appropriate in each case. In this way we found that, in general, we could use all frames with  $|HA| \leq 1.5$  hr.

Finally, having corrected the barycentric coordinates of all objects of interest for DCR, we redetermined the barycenter of the reference stars for all frames and therefore produced a new set of refraction-free barycentric coordinates.

### 3.4. Registration to the Standard Frame of Reference

The SFR is a reference system into which all images of a given QSO field (that is, the coordinates of all objects of interest in the field) are to be transformed. Measuring the position at different epochs of the background QSO with respect to the SFR leads in the end to the determination of the proper motion of the SMC stars in the field.

The SFR is defined by the DCR-corrected barycentric coordinates of bona fide SMC field stars. In practice, the SFR is established by averaging the coordinates of these reference stars in a set of consecutive, near meridian, good seeing images (usually three or four).

The construction of the SFR is an iterative process; we start with the set of stars that define the *initial* local reference system selected for each QSO field and progressively depurate it by eliminating objects that do not belong to the SMC or are problematic in any way.

The registration process itself is realized by means of a fourth-order geometrical transformation. Given that all images are taken placing the QSO within a few pixels of a chosen position, it involves only minor shifts, rotations, scale changes, and higher order optical distortions. Registration was done using a standard  $\chi^2$  minimization algorithm over a multiple nonlinear regression polynomial (adapted from Bevington 1969). We shall call these coordinates resulting from the registration process “standard coordinates.”

### 3.5. Cleansing of the Standard Frame of Reference

Save for residual motions, caused by positional uncertainties, uncertainties in the DCR correction and in the registration process, the standard coordinates of true SMC members will not change with time (assuming that our uncertainties are larger than any internal or streaming motion of the SMC stars).

This will not be the case of objects which do not conform to the SFR; therefore, plotting their standard coordinates as a function of epoch allows us to determine their motion with respect to the SFR (through a linear regression). If we apply this procedure to the stars that define the initial local reference system for a given QSO field, we can identify objects with large motions which must be excluded from the SFR.

Because the initial reference system is selected on a purely morphological way, some objects in it could be Galactic foreground stars (producing a true motion) and others could have hidden companions or other problems affecting the astrometry (which will produce a spurious motion). In an iterative process, high “motion” stars are removed, the SFR is re-defined, new standard coordinates are calculated, and thus new motions are determined. The cleansing process of the SFR is perhaps the most critical step in the whole procedure; up to the elimination of objects with motions larger than roughly  $1 \text{ mas yr}^{-1}$  the final result can change substantially. To put this value in perspective, we note that a Galactic halo field star with a velocity of  $120 \text{ km s}^{-1}$ , and at a distance of  $\sim 25 \text{ kpc}$ , will have a proper motion of  $1.0 \text{ mas yr}^{-1}$ ; therefore, by restricting the SFR members to stars with motions less than this value, we are minimizing the chance of contamination by Galactic foreground objects. Also, special care is taken to end up with a spatial distribution of stars as homogeneous as possible, centered on the corresponding QSOs. As shown by Figures 1–5 this was indeed the case.

It should be noted that in the final steps of the iteration process (i.e., after the removal of Galactic stars and problematic objects), we are dealing with motions whose magnitudes are of the order of their errors. This is evident in Tables 3–7 (where rounded numbers are given). These residual motions (see below) are most probably due to the various sources of error affecting the standard coordinates.

If the final SFR stars are true MC members, they will share a common motion—save for their internal velocity dispersion—consistent with zero with respect to the barycenter of the SFR, different from that of the background QSO. This is certainly the case, as shown by Figures 6, 7, 8, 9, and 10 which are residual (relative to the barycenter of the SFR) motion maps for the stars that define the SFR in fields QJ0033–7028, QJ0035–7201, QJ0047–7530, QJ0102–7546, and QJ0111–7249, respectively. We stress that the scatter seen on the SFR on these plots most probably stems entirely from random errors and *does not* represent the velocity dispersion in these MC fields.

For the sake of clarity, we have included only the error bars of the QSOs in Figures 6–10. These error bars represent the formal error of the slope in the straight-line fit to the barycentric position versus time diagrams presented in Figures 16–20 (see Section 3.6). We have adopted this value as a realistic estimate of our final proper motion errors, given that it includes *all* sources of positional uncertainty that contribute to the global scatter in the position versus epoch diagram (mainly centering uncertainties of the QSO at each epoch and registration uncertainties; uncertainties coming from the SFR itself are negligible). These errors are tabulated in Table 13 (see Section 3.7).



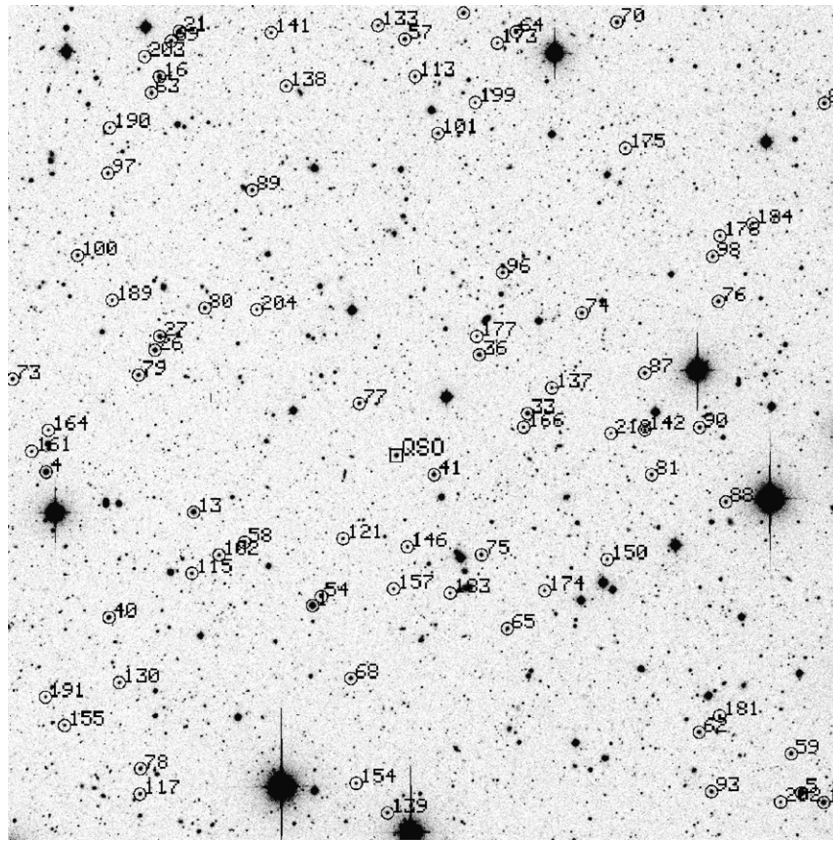


**Figure 1.** SMC field in the direction of the background quasar QJ0033–7028. The QSO is indicated by a square near the center of the field. The numbers identifying the reference stars (circles) are from our PEAK files. Image background has been conveniently altered. The size of the field is  $8.85 \times 8.85$  arcmin. North is at the top; east is to the left.

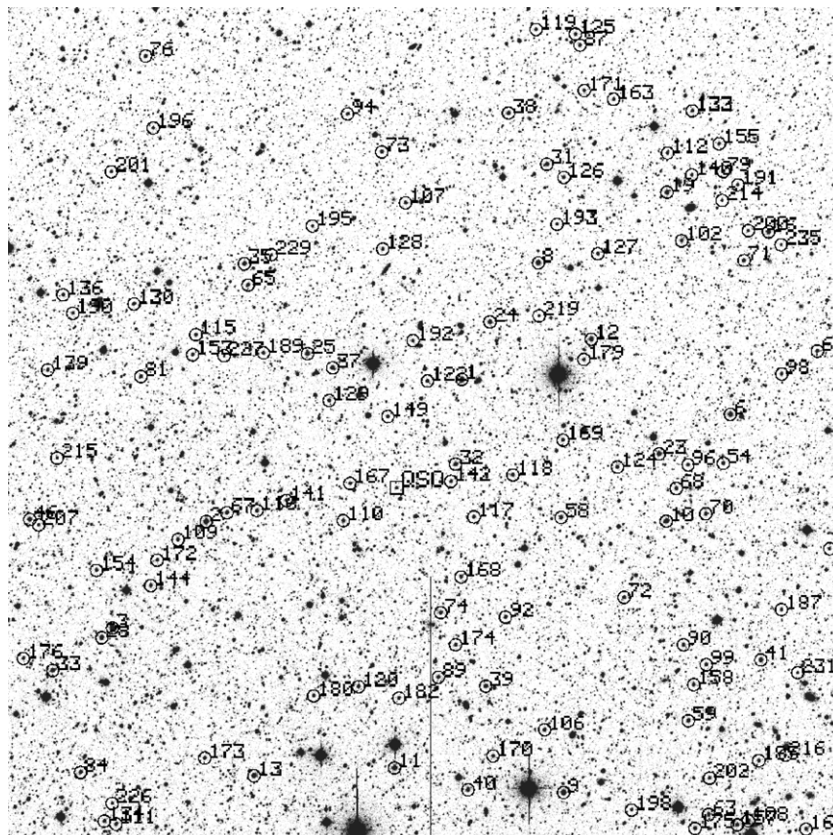


**Figure 2.** Same as Figure 1, for field QJ0035–7201.



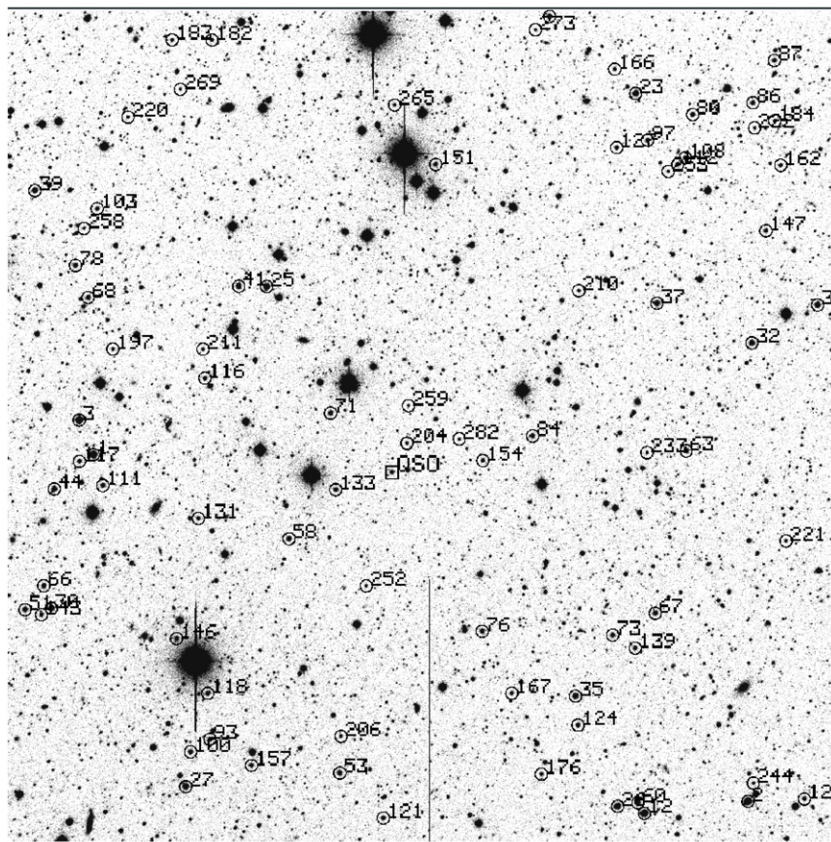


Figure 3. Same as Figure 1, for field QJ0047–7530.

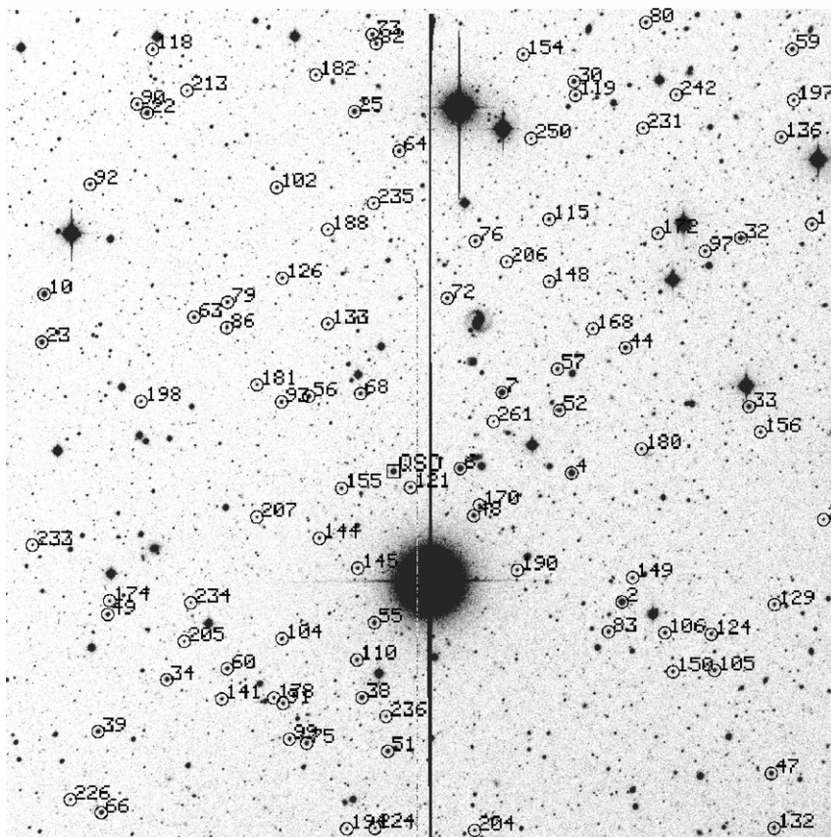


Figure 4. Same as Figure 1, for field QJ0102–7546.

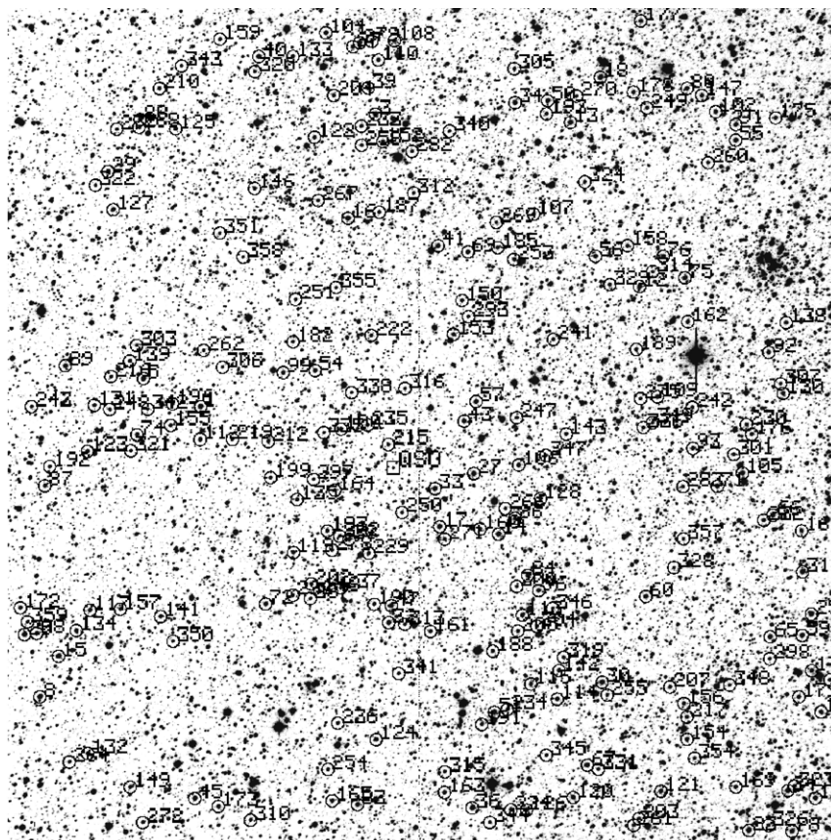


Figure 5. Same as Figure 1, for field QJ0111–7249.

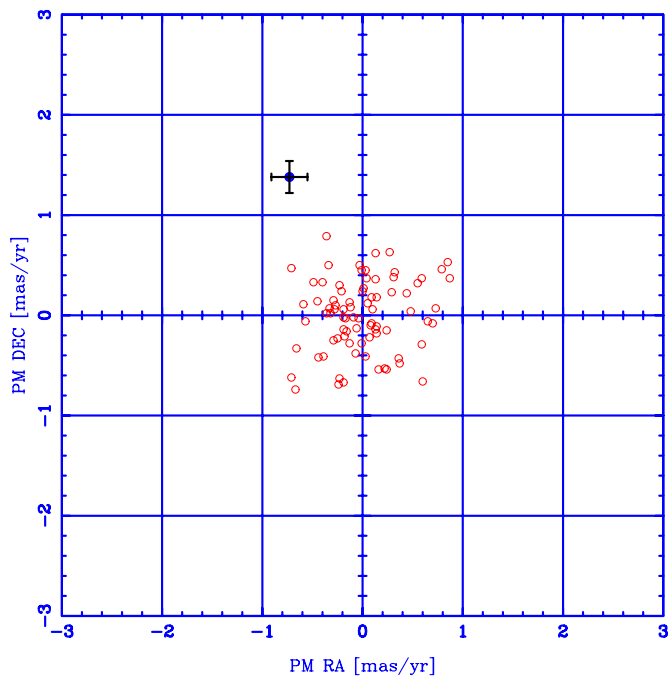


Figure 6. Residual motion map for the stars listed in Table 3, which defines the reference frame in the SMC field QJ0033–7028. The QSO is depicted by a filled circle with error bars. The weighted mean and error of the mean for the residual motions presented in Table 3 are  $-0.03 \pm 0.02$  mas yr $^{-1}$  in R.A. and  $+0.03 \pm 0.03$  mas yr $^{-1}$  in decl.

(A color version of this figure is available in the online journal.)

In Tables 3–7, we list the residual motions (relative to the barycenter of the field’s SFR), together with *calibrated*

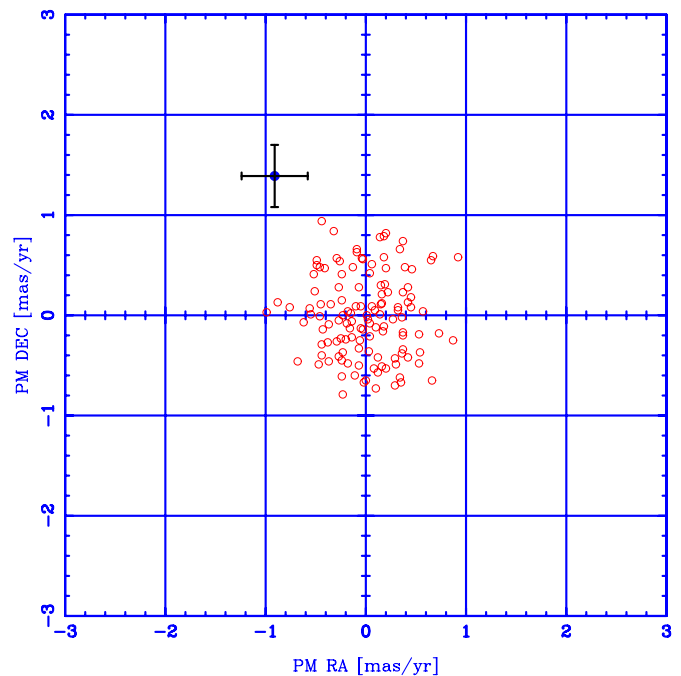


Figure 7. Same as Figure 6, for field QJ0035–7201. Stars are listed in Table 4. The weighted mean and error of the mean are  $+0.06 \pm 0.02$  mas yr $^{-1}$  in R.A. and  $-0.03 \pm 0.02$  mas yr $^{-1}$  in decl.

(A color version of this figure is available in the online journal.)

photometric data for the stars defining the local reference frame in each field (rounded numbers are given). Because the residual motions presented have similar errors (and there is



**Table 3**  
Local Reference Frame for the SMC Q0033–7028 Field

Star ID	$\mu_{\alpha} \cos \delta$ (mas yr <sup>-1</sup> )	$\sigma$ (mas yr <sup>-1</sup> )	$\mu_{\delta}$ (mas yr <sup>-1</sup> )	$\sigma$ (mas yr <sup>-1</sup> )	$R$ (mag)	$(B - R)$ (mag)
1	-0.3	0.3	0.0	0.2	16.83	1.71
4	-0.3	0.2	0.1	0.2	17.14	1.81
5	-0.2	0.1	0.2	0.2	17.16	1.60
13	-0.7	0.3	-0.6	0.3	17.61	1.68
16	0.3	0.1	0.4	0.2	17.86	1.48
19	0.0	0.2	-0.3	0.2	17.94	0.98
21	-0.3	0.2	0.1	0.2	17.96	1.59
26	0.0	0.2	0.0	0.1	18.13	1.53
27	-0.3	0.2	0.1	0.1	18.15	0.99
33	0.6	0.2	0.3	0.2	18.40	1.23
36	0.0	0.1	0.3	0.2	18.48	1.32
39	-0.2	0.2	-0.7	0.1	18.59	1.22
40	0.7	0.2	0.1	0.2	18.64	1.03
41	0.9	0.2	0.4	0.2	18.66	1.12
54	0.1	0.3	0.2	0.2	18.87	1.19
57	-0.5	0.1	0.3	0.3	18.91	1.35
58	-0.4	0.1	0.3	0.2	18.92	1.15
59	-0.2	0.2	0.1	0.2	18.97	1.30
62	-0.1	0.2	0.1	0.2	18.93	1.22
63	0.3	0.2	0.4	0.2	18.98	1.12
64	0.1	0.2	-0.2	0.2	18.95	1.17
65	0.4	0.3	0.2	0.2	18.98	1.26
68	0.0	0.3	0.4	0.3	18.99	1.11
69	-0.4	0.2	0.0	0.2	19.04	1.12
70	-0.3	0.2	0.5	0.3	19.04	1.35
73	0.0	0.2	0.2	0.2	19.03	1.17
74	0.1	0.2	0.6	0.3	18.99	1.05
75	0.2	0.2	-0.5	0.3	19.03	1.16
76	-0.1	0.1	-0.4	0.3	19.04	1.15
77	-0.7	0.2	-0.7	0.2	19.07	1.29
78	-0.2	0.3	0.0	0.2	19.03	1.16
79	0.0	0.2	-0.4	0.2	19.09	1.02
80	0.4	0.2	-0.4	0.2	19.06	1.06
81	-0.1	0.2	-0.1	0.2	19.08	1.13
85	0.1	0.2	0.2	0.1	19.22	1.20
87	0.0	0.2	0.5	0.3	19.15	1.26
88	0.7	0.2	-0.1	0.3	19.18	1.17
89	0.1	0.2	-0.1	0.3	19.17	1.12
90	-0.4	0.2	0.1	0.3	19.18	1.12
93	-0.2	0.2	0.0	0.2	19.23	1.15
96	-0.3	0.3	-0.2	0.3	19.31	0.88
97	-0.3	0.3	0.2	0.3	19.29	1.27
98	0.2	0.2	-0.5	0.2	19.36	1.16
100	0.0	0.2	0.4	0.3	19.36	1.24
101	-0.4	0.2	-0.4	0.3	19.37	1.24
102	-0.4	0.2	0.8	0.2	19.39	1.15
113	-0.6	0.2	0.1	0.2	19.56	1.16
115	0.9	0.2	0.5	0.2	19.65	0.63
117	-0.2	0.3	-0.1	0.3	19.67	1.02
121	0.1	0.3	-0.2	0.3	19.76	1.11
130	0.1	0.3	-0.1	0.3	19.86	1.21
133	0.8	0.3	0.5	0.2	19.87	0.69
137	-0.7	0.4	0.5	0.3	20.05	1.19
138	0.1	0.3	0.4	0.2	19.97	1.26
139	0.1	0.3	-0.1	0.2	19.97	1.11
141	0.2	0.4	-0.2	0.3	20.02	1.12
142	0.1	0.3	0.1	0.4	20.03	1.25
146	0.4	0.3	-0.5	0.4	20.13	1.22
150	-0.2	0.4	-0.7	0.4	20.11	1.19
154	0.0	0.3	0.1	0.3	20.13	1.18
155	0.3	0.5	0.2	0.3	20.31	1.28
157	-0.1	0.3	-0.3	0.3	20.21	1.21
161	-0.2	0.3	-0.2	0.3	20.26	1.15
164	0.1	0.4	-0.1	0.4	20.29	1.15
166	-0.1	0.3	0.0	0.3	20.31	1.18

**Table 3**  
(Continued)

Star ID	$\mu_{\alpha} \cos \delta$ (mas yr <sup>-1</sup> )	$\sigma$ (mas yr <sup>-1</sup> )	$\mu_{\delta}$ (mas yr <sup>-1</sup> )	$\sigma$ (mas yr <sup>-1</sup> )	$R$ (mag)	$(B - R)$ (mag)
173	0.6	0.3	-0.3	0.3	20.36	1.09
174	-0.7	0.3	-0.3	0.4	20.35	1.19
175	0.6	0.4	-0.7	0.4	20.32	1.11
177	0.3	0.3	0.6	0.3	20.38	1.03
178	-0.6	0.3	-0.1	0.4	20.43	1.21
181	-0.2	0.3	0.3	0.3	20.39	1.20
183	-0.4	0.5	-0.4	0.4	20.51	1.21
184	-0.1	0.3	0.1	0.3	20.45	1.15
189	0.5	0.3	0.0	0.3	20.48	1.08
190	0.2	0.4	-0.5	0.5	20.55	0.60
191	-0.3	0.5	-0.3	0.3	20.59	1.19
199	0.0	0.5	0.4	0.3	20.63	1.14
202	0.6	0.4	-0.1	0.4	20.83	0.79
203	-0.2	0.3	-0.6	0.4	20.56	0.89
204	-0.2	0.6	-0.2	0.5	20.77	1.00
218	0.6	0.7	0.4	0.5	20.86	1.15

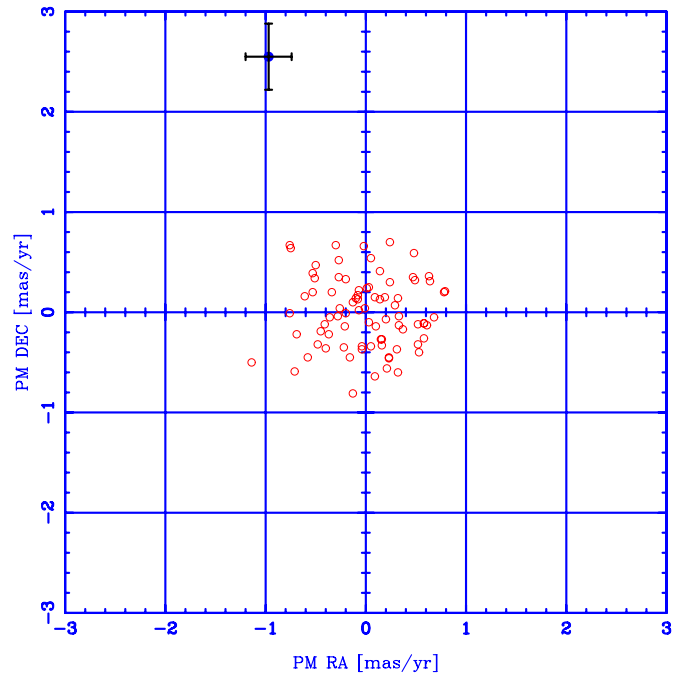


**Figure 8.** Same as Figure 6, for field QJ0047–7530. Stars are listed in Table 5. The weighted mean and error of the mean are  $+0.01 \pm 0.02$  mas yr<sup>-1</sup> in R.A. and  $-0.04 \pm 0.03$  mas yr<sup>-1</sup> in decl.

(A color version of this figure is available in the online journal.)

no evidence for systematic effects), it makes sense to determine their weighted mean and its error, which turn out to be (following Bevington 1969):  $-0.03 \pm 0.02$  mas yr<sup>-1</sup> in R.A. and  $+0.03 \pm 0.03$  mas yr<sup>-1</sup> in decl. (QJ0033–7028,  $N_{\text{stars}} = 81$ ),  $+0.006 \pm 0.02$  mas yr<sup>-1</sup> in R.A. and  $-0.03 \pm 0.02$  mas yr<sup>-1</sup> in decl. (QJ0035–7201,  $N_{\text{stars}} = 126$ ),  $+0.01 \pm 0.02$  mas yr<sup>-1</sup> in R.A. and  $-0.04 \pm 0.03$  mas yr<sup>-1</sup> in decl. (QJ0047–7530,  $N_{\text{stars}} = 82$ ),  $-0.02 \pm 0.02$  mas yr<sup>-1</sup> in R.A. and  $-0.008 \pm 0.03$  mas yr<sup>-1</sup> in decl. (QJ0102–7546,  $N_{\text{stars}} = 98$ ), and  $-0.02 \pm 0.01$  mas yr<sup>-1</sup> in R.A. and  $+0.03 \pm 0.01$  mas yr<sup>-1</sup> in decl. (QJ0111–7249,  $N_{\text{stars}} = 243$ ).

As mentioned above, uncertainties inherent to the SFR are negligible, which can be clearly seen by comparing the above

**Table 4**  
Local Reference Frame for the SMC Q0035–7201 Field

Star ID	$\mu_{\alpha} \cos \delta$ (mas yr <sup>-1</sup> )	$\sigma$ (mas yr <sup>-1</sup> )	$\mu_{\delta}$ (mas yr <sup>-1</sup> )	$\sigma$ (mas yr <sup>-1</sup> )	$R$ (mag)	$(B - R)$ (mag)
1	0.7	0.1	0.6	0.3	17.41	2.64
2	0.0	0.2	-0.4	0.3	17.56	2.39
3	0.4	0.1	0.0	0.2	17.58	2.61
6	-0.1	0.2	0.5	0.2	17.68	2.53
8	0.0	0.1	-0.6	0.3	17.79	2.45
9	0.5	0.2	-0.2	0.2	17.86	2.54
10	0.3	0.1	-0.6	0.3	17.88	2.22
11	0.3	0.1	0.1	0.1	17.92	2.38
12	-0.5	0.1	0.5	0.2	17.99	2.49
13	-0.6	0.2	-0.1	0.1	18.01	2.34
16	0.3	0.1	0.0	0.1	18.02	2.29
19	-0.1	0.2	-0.6	0.2	18.12	2.36
23	0.2	0.2	0.3	0.3	18.16	2.42
24	-0.1	0.1	0.3	0.2	18.16	2.27
25	0.1	0.1	0.0	0.2	18.23	2.20
28	0.5	0.1	-0.4	0.2	18.33	2.32
31	-0.4	0.1	-0.3	0.2	18.41	1.48
32	0.2	0.3	0.3	0.2	18.44	2.11
33	-0.1	0.2	-0.5	0.2	18.47	2.23
35	0.2	0.1	0.2	0.2	18.48	2.27
37	-0.4	0.2	-0.5	0.2	18.54	2.22
38	-0.3	0.2	0.5	0.1	18.52	1.88
39	0.2	0.2	-0.2	0.2	18.53	2.24
40	0.1	0.4	-0.4	0.1	18.55	2.21
41	0.3	0.2	-0.7	0.2	18.58	2.25
46	0.4	0.2	-0.3	0.2	18.77	2.19
54	0.3	0.2	0.7	0.3	18.89	2.16
58	-0.4	0.3	-0.4	0.4	18.94	1.88
59	-0.4	0.2	0.5	0.2	18.95	2.04
63	-0.4	0.2	0.1	0.1	18.98	1.91
65	0.1	0.2	-0.7	0.3	19.02	2.17
67	-0.1	0.1	-0.3	0.3	19.00	2.22
68	0.1	0.2	-0.5	0.2	19.04	2.11
69	-0.5	0.2	0.2	0.2	19.03	2.03
70	0.4	0.2	-0.2	0.2	19.05	2.12
71	0.9	0.2	-0.3	0.2	19.04	1.78
72	-0.2	0.2	-0.1	0.3	19.04	1.91
73	0.4	0.1	0.2	0.2	19.04	2.16
74	-0.5	0.2	-0.5	0.2	19.05	2.14
76	-0.3	0.2	-0.3	0.2	19.06	1.90
79	0.0	0.2	-0.1	0.1	19.16	2.12
81	0.7	0.3	-0.6	0.2	19.19	2.13
84	0.3	0.3	0.0	0.2	19.16	1.92
87	-0.4	0.1	-0.1	0.1	19.23	2.08
89	0.0	0.2	-0.1	0.2	19.24	1.89
90	0.4	0.3	0.2	0.2	19.24	2.14
92	-0.5	0.2	0.0	0.2	19.22	2.00
94	0.6	0.2	0.6	0.2	19.24	1.99
96	0.4	0.2	-0.2	0.3	19.27	1.94
98	-0.2	0.1	0.0	0.2	19.25	1.89
99	0.6	0.3	0.0	0.2	19.27	1.90
102	0.0	0.3	-0.7	0.2	19.31	2.07
106	0.2	0.2	0.8	0.3	19.29	1.95
107	-0.2	0.2	-0.6	0.2	19.39	1.96
108	-0.2	0.2	-0.8	0.3	19.35	1.99
109	-0.5	0.2	0.4	0.3	19.31	2.11
110	0.4	0.4	-0.4	0.3	19.34	1.98
111	-0.3	0.2	0.0	0.2	19.40	1.92
112	-0.2	0.2	0.4	0.2	19.35	1.92
115	0.1	0.2	0.0	0.2	19.32	2.14
116	-0.1	0.2	-0.3	0.2	19.36	2.15
117	-0.2	0.1	-0.1	0.2	19.35	1.26
118	0.7	0.2	-0.2	0.2	19.38	1.99

**Table 4**  
(Continued)

Star ID	$\mu_{\alpha} \cos \delta$ (mas yr <sup>-1</sup> )	$\sigma$ (mas yr <sup>-1</sup> )	$\mu_{\delta}$ (mas yr <sup>-1</sup> )	$\sigma$ (mas yr <sup>-1</sup> )	$R$ (mag)	$(B - R)$ (mag)
119	0.3	0.2	-0.7	0.2	19.34	1.90
120	0.0	0.3	0.1	0.3	19.37	1.90
122	0.1	0.2	0.8	0.3	19.36	1.93
124	-0.9	0.2	0.1	0.3	19.39	1.96
125	0.0	0.2	-0.1	0.1	19.36	1.88
126	0.0	0.2	-0.2	0.2	19.38	1.93
127	0.3	0.2	-0.5	0.3	19.39	1.82
128	-0.7	0.2	-0.5	0.2	19.39	2.01
129	-0.2	0.2	-0.4	0.2	19.41	1.97
130	0.4	0.2	0.5	0.3	19.38	1.97
133	0.2	0.2	0.2	0.3	19.39	1.84
134	0.0	0.1	0.0	0.2	19.39	1.86
136	-0.1	0.2	-0.1	0.2	19.39	1.92
139	-0.2	0.2	-0.4	0.2	19.46	2.13
140	0.1	0.2	-0.1	0.2	19.40	1.94
141	0.1	0.3	-0.6	0.3	19.42	2.13
142	0.4	0.2	0.3	0.2	19.40	1.98
144	-0.4	0.2	0.9	0.2	19.41	1.96
149	-0.3	0.1	0.1	0.2	19.42	1.94
153	-0.1	0.2	0.1	0.2	19.42	1.88
154	-0.1	0.2	0.6	0.2	19.42	2.16
155	-0.3	0.2	0.8	0.2	19.47	1.98
157	0.2	0.1	-0.5	0.2	19.44	1.99
158	-0.3	0.2	0.3	0.2	19.48	2.13
163	0.5	0.2	0.5	0.3	19.50	1.92
164	0.9	0.3	0.6	0.3	19.49	1.95
167	0.4	0.2	0.1	0.2	19.50	1.94
168	-0.2	0.2	0.0	0.3	19.54	1.84
169	-0.6	0.2	0.0	0.3	19.49	2.06
170	0.2	0.4	0.5	0.2	19.51	1.86
171	0.0	0.2	0.6	0.2	19.50	2.10
172	0.2	0.2	0.8	0.2	19.50	1.97
173	0.5	0.2	-0.5	0.2	19.52	1.92
174	0.4	0.2	-0.4	0.2	19.50	1.85
175	-0.4	0.2	-0.1	0.2	19.49	1.93
176	-0.3	0.2	-0.2	0.2	19.49	1.96
179	-0.3	0.2	0.6	0.3	19.51	1.96
180	-1.0	0.2	0.0	0.3	19.51	2.11
182	0.4	0.2	0.1	0.3	19.54	1.87
185	-0.4	0.2	-0.3	0.2	19.59	1.95
187	0.3	0.2	-0.4	0.2	19.55	1.96
189	-0.1	0.2	-0.2	0.2	19.58	1.99
190	0.2	0.2	0.1	0.2	19.63	1.88
191	-0.2	0.2	-0.2	0.2	19.71	1.94
192	0.2	0.3	0.6	0.3	19.74	2.05
193	-0.2	0.2	-0.5	0.2	19.69	1.55
195	-0.2	0.2	0.0	0.2	19.76	2.05
196	0.0	0.2	0.4	0.2	19.78	0.97
197	-0.5	0.2	0.5	0.3	19.77	2.02
198	0.0	0.2	0.6	0.3	19.78	2.18
200	0.2	0.2	-0.1	0.2	19.89	2.03
201	0.0	0.2	0.0	0.3	19.93	2.00
202	-0.6	0.3	0.1	0.2	19.83	1.61
207	-0.5	0.2	0.6	0.3	20.07	2.00
214	-0.2	0.3	0.2	0.3	20.25	2.18
215	0.2	0.3	0.1	0.3	20.29	1.99
216	-0.1	0.3	0.7	0.3	20.29	1.99
219	0.4	0.2	0.7	0.4	20.25	1.15
226	0.1	0.3	0.5	0.3	20.47	1.98
227	-0.8	0.3	0.1	0.3	20.49	1.96
229	0.1	0.3	0.1	0.3	20.54	1.90
231	-0.3	0.3	-0.4	0.4	20.58	1.98
235	0.2	0.3	-0.5	0.3	20.72	1.90



**Table 5**  
Local Reference Frame for the SMC Q0047–7530 Field

Star ID	$\mu_{\alpha} \cos \delta$ (mas yr <sup>-1</sup> )	$\sigma$ (mas yr <sup>-1</sup> )	$\mu_{\delta}$ (mas yr <sup>-1</sup> )	$\sigma$ (mas yr <sup>-1</sup> )	$R$ (mag)	$(B - R)$ (mag)
1	-0.1	0.2	0.0	0.2	16.64	2.01
2	-0.4	0.3	-0.2	0.2	16.66	1.99
3	-0.1	0.3	-0.8	0.3	16.63	1.98
12	-0.4	0.2	-0.1	0.1	17.01	1.95
23	0.4	0.2	-0.2	0.2	17.49	1.75
25	0.2	0.2	-0.5	0.2	17.56	1.67
26	0.1	0.1	-0.1	0.1	17.58	1.70
27	0.0	0.2	0.5	0.3	17.62	1.80
30	0.2	0.2	-0.1	0.1	17.68	1.58
31	0.3	0.2	0.0	0.2	17.74	1.42
32	-0.2	0.2	0.3	0.2	17.75	1.68
35	-0.2	0.1	0.0	0.2	17.91	1.57
37	0.3	0.2	0.1	0.4	17.90	1.67
39	0.3	0.3	0.1	0.2	18.00	1.11
41	0.6	0.2	-0.1	0.3	18.03	1.35
44	-0.5	0.2	0.2	0.2	18.15	1.18
48	0.1	0.4	0.4	0.4	18.29	1.35
51	0.1	0.1	0.2	0.1	18.39	1.38
53	-0.2	0.2	-0.3	0.2	18.43	1.49
58	0.0	0.2	0.7	0.3	18.55	1.21
60	-0.2	0.2	-0.1	0.1	18.56	1.21
63	0.0	0.2	-0.3	0.4	18.58	1.49
66	0.2	0.1	-0.3	0.2	18.65	1.22
67	0.3	0.2	-0.6	0.3	18.66	1.69
68	0.5	0.2	0.3	0.2	18.66	1.11
71	-0.7	0.2	-0.6	0.3	18.69	1.24
73	-0.7	0.2	-0.2	0.3	18.70	1.35
76	0.6	0.3	-0.3	0.3	18.75	1.40
78	-0.8	0.2	0.0	0.2	18.78	1.41
80	0.5	0.1	-0.3	0.2	18.79	1.19
84	-0.6	0.3	0.2	0.2	18.88	1.43
86	-0.5	0.2	0.3	0.2	18.88	1.21
87	0.2	0.2	-0.4	0.3	18.90	1.44
90	0.2	0.2	0.2	0.2	18.93	1.19
93	0.0	0.2	-0.4	0.2	18.98	1.14
97	0.6	0.2	0.3	0.3	19.00	1.17
100	-0.1	0.2	0.1	0.2	19.03	1.23
103	-0.1	0.3	0.2	0.3	19.03	1.39
108	0.1	0.2	0.1	0.2	19.05	1.19
111	0.0	0.2	0.0	0.2	19.08	1.17
112	0.2	0.2	-0.3	0.2	19.09	1.21
116	0.3	0.3	-0.4	0.2	19.06	1.21
117	-0.4	0.2	-0.2	0.3	19.08	1.21
118	-0.6	0.2	-0.4	0.2	19.12	1.24
121	0.6	0.3	-0.1	0.2	19.10	1.09
124	0.2	0.2	0.7	0.3	19.12	1.25
127	0.5	0.2	-0.4	0.3	19.15	1.23
128	0.7	0.3	0.0	0.2	19.15	1.40
131	-0.3	0.3	0.7	0.4	19.15	1.10
133	0.2	0.3	0.3	0.3	19.22	1.28
139	-0.3	0.2	0.3	0.2	19.22	1.24
143	0.3	0.3	-0.1	0.3	19.37	1.26
146	0.5	0.3	0.6	0.3	19.34	1.22
147	-0.1	0.2	0.1	0.3	19.36	1.40
151	-1.1	0.3	-0.5	0.3	19.42	1.02
154	0.6	0.3	-0.1	0.3	19.43	0.94
157	-0.4	0.3	0.0	0.2	19.55	1.29
162	-0.3	0.2	0.2	0.3	19.62	1.35
166	-0.3	0.3	0.0	0.3	19.64	1.35
167	0.8	0.3	0.2	0.2	19.67	0.52
176	0.6	0.3	0.4	0.2	19.80	1.32
182	0.0	0.4	0.3	0.3	19.84	1.29
183	-0.2	0.2	-0.4	0.2	19.85	1.31
184	-0.5	0.3	0.4	0.3	19.88	1.31
197	0.5	0.5	-0.1	0.3	19.95	1.29

**Table 5**  
(Continued)

Star ID	$\mu_{\alpha} \cos \delta$ (mas yr <sup>-1</sup> )	$\sigma$ (mas yr <sup>-1</sup> )	$\mu_{\delta}$ (mas yr <sup>-1</sup> )	$\sigma$ (mas yr <sup>-1</sup> )	$R$ (mag)	$(B - R)$ (mag)
204	-0.1	0.4	0.1	0.3	20.09	1.28
206	-0.5	0.4	-0.3	0.4	20.15	1.30
210	-0.8	0.4	0.7	0.4	20.16	1.24
211	0.8	0.4	0.2	0.4	20.10	1.22
220	0.1	0.4	-0.6	0.5	20.23	1.23
221	0.2	0.4	-0.3	0.4	20.28	1.24
222	0.0	0.4	-0.1	0.4	20.31	0.99
233	-0.1	0.5	0.2	0.6	20.37	0.34
244	-0.5	0.8	0.5	0.6	20.70	0.75
252	-0.4	0.4	-0.4	0.4	20.48	1.22
253	0.2	0.5	-0.6	0.4	20.63	1.21
258	-0.8	0.5	0.6	0.6	20.67	1.21
259	0.0	0.4	0.2	0.5	20.62	1.22
265	-0.3	0.4	0.5	0.4	20.68	0.20
269	0.5	0.6	0.3	0.6	20.90	1.19
273	-0.3	0.5	0.0	0.4	20.84	1.17
282	0.0	0.6	-0.3	0.5	20.87	1.06

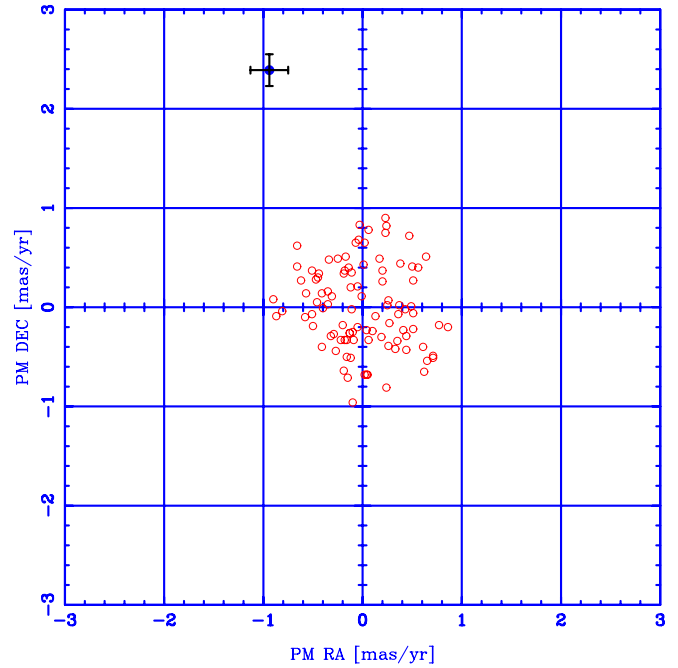


**Figure 9.** Same as Figure 6, for field QJ0102–7546. Stars are listed in Table 6. The weighted mean and error of the mean are  $-0.02 \pm 0.02$  mas yr<sup>-1</sup> in R.A. and  $-0.008 \pm 0.03$  mas yr<sup>-1</sup> in decl.

(A color version of this figure is available in the online journal.)

values of the mean motion and its uncertainty for each SFR, with those derived using an unweighted mean, which are  $+0.000 \pm 0.042$  mas yr<sup>-1</sup> in R.A. and  $+0.000 \pm 0.040$  mas yr<sup>-1</sup> in decl. (QJ0033–7028,  $N_{\text{stars}} = 81$ ),  $+0.000 \pm 0.033$  mas yr<sup>-1</sup> in R.A. and  $+0.000 \pm 0.037$  mas yr<sup>-1</sup> in decl. (QJ0035–7201,  $N_{\text{stars}} = 126$ ),  $+0.002 \pm 0.046$  mas yr<sup>-1</sup> in R.A. and  $-0.001 \pm 0.039$  mas yr<sup>-1</sup> in decl. (QJ0047–7530,  $N_{\text{stars}} = 82$ ),  $+0.000 \pm 0.040$  mas yr<sup>-1</sup> in R.A. and  $-0.001 \pm 0.043$  mas yr<sup>-1</sup> in decl. (QJ0102–7546,  $N_{\text{stars}} = 98$ ), and  $-0.002 \pm 0.024$  mas yr<sup>-1</sup> in R.A. and  $-0.001 \pm 0.028$  mas yr<sup>-1</sup> in decl. (QJ0111–7249,  $N_{\text{stars}} = 243$ ). The rms scatter of the SFR stars, which is indicative of the typical uncertainty in the proper motion of any of them, is  $0.376$  mas yr<sup>-1</sup> in R.A. and  $0.356$  mas yr<sup>-1</sup> in decl. (QJ0033–7028,  $N_{\text{stars}} = 81$ ),  $0.366$  mas yr<sup>-1</sup> in

**Table 6**  
Local Reference Frame for the SMC Q0102–7546 Field

Star ID	$\mu_{\alpha} \cos \delta$ (mas yr <sup>-1</sup> )	$\sigma$ (mas yr <sup>-1</sup> )	$\mu_{\delta}$ (mas yr <sup>-1</sup> )	$\sigma$ (mas yr <sup>-1</sup> )	$R$ (mag)	$(B - R)$ (mag)
2	-0.2	0.2	-0.7	0.2	16.61	1.94
4	-0.1	0.2	-1.0	0.2	16.73	2.08
6	0.5	0.2	0.4	0.1	16.92	1.73
7	0.0	0.1	0.6	0.3	16.97	1.93
10	-0.4	0.1	0.0	0.3	17.08	1.83
22	0.5	0.2	-0.1	0.2	17.55	1.52
23	0.3	0.2	-0.2	0.3	17.62	0.95
25	0.3	0.2	0.1	0.2	17.73	1.62
30	0.4	0.1	-0.1	0.2	17.91	1.05
32	-0.3	0.2	-0.3	0.2	17.98	-0.18
33	-0.2	0.2	0.3	0.2	18.06	1.50
34	0.7	0.2	-0.5	0.2	18.08	1.57
38	0.0	0.2	0.4	0.2	18.19	1.45
39	0.6	0.2	-0.5	0.2	18.19	1.54
44	-0.3	0.1	0.0	0.2	18.31	1.28
47	-0.6	0.2	0.1	0.2	18.41	1.17
48	-0.2	0.2	-0.2	0.2	18.43	-0.13
49	-0.1	0.3	0.2	0.2	18.41	1.15
51	0.2	0.2	0.5	0.2	18.45	1.35
52	0.2	0.2	0.8	0.3	18.47	1.39
55	-0.1	0.1	-0.3	0.2	18.49	1.02
56	-0.1	0.2	-0.5	0.2	18.55	1.43
57	0.0	0.2	0.7	0.3	18.57	1.44
59	0.0	0.3	-0.2	0.3	18.57	1.43
60	-0.5	0.1	0.4	0.2	18.58	1.13
63	0.6	0.2	0.4	0.2	18.61	1.22
64	0.6	0.2	0.5	0.2	18.60	1.35
66	-0.2	0.3	0.5	0.3	18.64	1.21
68	-0.9	0.2	-0.1	0.2	18.67	1.09
72	0.0	0.2	-0.7	0.2	18.74	1.14
73	-0.3	0.2	-0.4	0.3	18.74	1.47
75	-0.3	0.2	0.1	0.2	18.73	1.32
76	-0.3	0.2	-0.3	0.2	18.82	1.24
79	0.3	0.2	-0.3	0.2	18.87	1.28
80	-0.2	0.3	0.4	0.3	18.87	1.36
82	-0.5	0.2	0.0	0.3	18.89	1.15
83	-0.6	0.2	0.3	0.2	18.88	1.47
86	-0.7	0.2	0.6	0.3	18.93	1.16
90	0.5	0.2	0.0	0.2	18.91	1.41
91	-0.6	0.2	-0.1	0.2	18.93	-0.03
92	-0.2	0.2	-0.3	0.3	18.97	1.45
93	-0.2	0.2	-0.3	0.3	18.99	1.10
97	0.4	0.2	-0.3	0.2	19.08	1.22
99	-0.1	0.2	-0.3	0.2	19.06	1.19
102	0.1	0.2	0.8	0.3	19.09	1.13
104	-0.4	0.2	0.3	0.3	19.11	1.39
105	0.4	0.2	-0.2	0.2	19.12	1.14
106	0.4	0.2	0.0	0.2	19.16	-0.03
110	-0.1	0.2	-0.3	0.2	19.15	1.19
115	-0.2	0.2	-0.6	0.3	19.20	1.00
118	-0.1	0.2	0.0	0.3	19.26	1.19
119	-0.4	0.2	0.1	0.2	19.21	1.18
121	0.2	0.3	0.8	0.2	19.26	1.30
124	-0.1	0.4	0.4	0.3	19.34	1.28
126	-0.3	0.2	0.5	0.2	19.36	1.12
129	0.6	0.3	-0.6	0.3	19.30	1.19
132	0.3	0.1	0.0	0.2	19.37	1.22
133	-0.8	0.3	0.0	0.3	19.34	1.30
136	-0.5	0.2	0.3	0.3	19.37	1.23
138	0.5	0.3	-0.2	0.3	19.41	0.18
141	-0.5	0.2	-0.2	0.2	19.43	0.80
144	0.6	0.3	-0.4	0.3	19.45	1.16
145	0.3	0.3	-0.4	0.3	19.49	0.10
148	0.5	0.3	0.3	0.3	19.77	0.74
149	-0.2	0.3	-0.5	0.3	19.57	1.19

**Table 6**  
(Continued)

Star ID	$\mu_{\alpha} \cos \delta$ (mas yr <sup>-1</sup> )	$\sigma$ (mas yr <sup>-1</sup> )	$\mu_{\delta}$ (mas yr <sup>-1</sup> )	$\sigma$ (mas yr <sup>-1</sup> )	$R$ (mag)	$(B - R)$ (mag)
150	-0.1	0.3	0.3	0.2	19.56	1.32
154	0.8	0.3	-0.2	0.3	19.60	1.15
155	0.9	0.2	-0.2	0.4	19.58	1.27
156	0.4	0.3	0.4	0.4	19.58	1.32
168	-0.5	0.3	-0.1	0.3	19.88	-0.03
170	0.4	0.3	0.0	0.4	19.95	1.16
172	0.4	0.3	-0.4	0.3	19.93	0.15
174	-0.3	0.3	0.5	0.4	19.98	1.27
178	0.0	0.5	0.2	0.3	19.96	1.14
180	-0.9	0.3	0.1	0.5	20.02	1.18
181	0.2	0.4	0.4	0.4	20.03	0.17
182	0.2	0.4	-0.3	0.3	20.01	0.19
188	-0.2	0.3	-0.3	0.5	20.05	0.66
190	0.3	0.4	-0.4	0.3	20.05	0.10
194	0.1	0.3	-0.1	0.3	20.10	1.19
197	0.0	0.3	0.1	0.3	20.07	1.17
198	0.7	0.4	-0.5	0.4	20.23	0.10
204	0.1	0.4	-0.2	0.4	20.30	1.06
205	0.0	0.3	0.8	0.4	20.20	0.24
206	0.0	0.4	-0.7	0.6	20.30	1.25
207	0.0	0.5	-0.7	0.6	20.18	1.24
213	-0.7	0.4	0.4	0.3	20.35	1.19
224	0.0	0.4	-0.2	0.4	20.40	0.15
226	0.1	0.4	-0.3	0.3	20.42	0.92
231	-0.1	0.6	0.6	0.6	20.53	1.22
233	-0.4	0.3	0.3	0.7	20.56	0.87
234	0.2	0.5	-0.8	0.6	20.54	1.16
235	-0.4	0.5	-0.4	0.5	20.52	0.37
236	0.5	0.4	0.7	0.5	20.51	0.08
242	-0.1	0.5	-0.3	0.5	20.40	0.16
250	0.2	0.4	0.3	0.6	20.52	0.33
252	-0.3	0.4	0.2	0.3	20.62	0.32
261	0.2	0.5	0.9	0.6	20.72	0.13

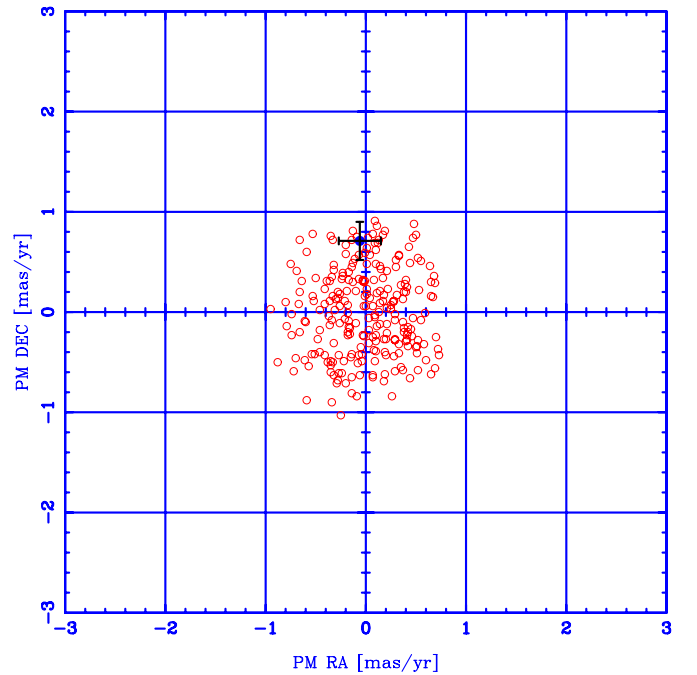


**Figure 10.** Same as Figure 6, for field QJ0111–7249. Stars are listed in Table 7. The weighted mean and error of the mean are  $-0.02 \pm 0.01$  mas yr<sup>-1</sup> in R.A. and  $+0.03 \pm 0.01$  mas yr<sup>-1</sup> in decl.

(A color version of this figure is available in the online journal.)

**Table 7**  
Local Reference Frame for the SMC Q0111–7249 Field

Star ID	$\mu_{\alpha} \cos \delta$ (mas yr <sup>-1</sup> )	$\sigma$ (mas yr <sup>-1</sup> )	$\mu_{\delta}$ (mas yr <sup>-1</sup> )	$\sigma$ (mas yr <sup>-1</sup> )	$R$ (mag)	$(B - R)$ (mag)
1	-0.6	0.3	-0.9	0.2	16.66	1.48
3	0.5	0.1	-0.3	0.1	16.74	-0.15
5	0.3	0.2	0.1	0.2	16.75	1.97
8	-0.3	0.1	-0.1	0.1	16.83	1.79
9	0.0	0.1	0.1	0.3	16.84	1.90
12	0.3	0.1	-0.4	0.3	16.89	1.69
13	-0.3	0.2	-0.3	0.2	16.88	1.47
14	-0.3	0.1	-0.5	0.2	16.89	0.95
15	-0.1	0.2	-0.4	0.2	16.88	1.93
16	-0.4	0.1	-0.5	0.2	16.88	-0.18
17	0.5	0.2	-0.1	0.1	16.89	1.83
18	0.0	0.1	0.3	0.2	16.92	1.57
20	0.6	0.1	-0.3	0.3	16.97	1.86
23	-0.9	0.2	-0.5	0.3	16.97	-0.05
24	0.1	0.1	0.5	0.1	16.97	1.63
25	-0.3	0.1	-0.5	0.2	17.01	1.56
27	0.4	0.2	0.5	0.2	17.02	1.86
29	0.1	0.1	0.3	0.3	16.99	1.94
30	-0.2	0.1	0.7	0.1	17.02	1.75
31	0.1	0.2	0.1	0.2	17.11	1.67
32	0.1	0.1	-0.6	0.2	17.08	1.80
33	0.5	0.2	0.5	0.2	17.09	1.76
34	0.0	0.1	0.6	0.2	17.10	1.18
36	0.7	0.4	-0.4	0.2	17.20	1.37
38	0.4	0.3	-0.2	0.2	17.09	0.82
39	0.0	0.1	-0.1	0.1	17.19	0.94
40	0.2	0.3	-0.3	0.1	17.19	1.34
41	-0.6	0.1	-0.5	0.1	17.20	-0.30
43	0.7	0.2	0.4	0.3	17.25	1.69
45	0.1	0.3	0.0	0.1	17.21	1.89
47	-0.1	0.1	-0.8	0.2	17.30	0.86
50	0.3	0.1	-0.1	0.2	17.24	0.63
51	0.3	0.3	0.4	0.1	17.29	1.41
54	-0.3	0.2	0.1	0.1	17.28	-0.06
55	-0.6	0.1	-0.1	0.2	17.28	0.60
56	0.5	0.1	-0.2	0.2	17.34	1.87
57	0.5	0.1	0.7	0.2	17.31	1.78
59	-0.3	0.1	-0.7	0.2	17.34	1.07
60	0.4	0.1	0.2	0.2	17.36	-0.11
65	0.5	0.2	-0.6	0.1	17.38	0.88
66	0.4	0.1	0.6	0.3	17.45	1.45
67	-0.1	0.2	0.8	0.1	17.47	0.00
69	-0.8	0.1	-0.1	0.2	17.44	1.20
71	0.5	0.2	-0.4	0.3	17.52	1.48
72	-0.7	0.2	0.7	0.3	17.49	0.92
74	0.4	0.1	-0.7	0.2	17.51	-0.30
75	0.4	0.2	-0.3	0.3	17.59	-0.27
76	0.4	0.2	-0.2	0.3	17.50	1.77
78	0.3	0.1	0.2	0.4	17.53	1.70
79	-0.1	0.1	0.3	0.3	17.52	0.59
80	0.1	0.2	-0.3	0.3	17.57	-0.27
83	-0.3	0.1	-0.6	0.2	17.57	1.09
84	-0.1	0.2	-0.8	0.3	17.61	1.01
86	-0.1	0.1	-0.5	0.2	17.66	1.69
87	-0.6	0.2	0.3	0.2	17.64	1.42
88	0.0	0.2	0.2	0.1	17.59	1.05
89	-0.1	0.4	0.4	0.3		
91	0.0	0.1	-0.2	0.1	17.61	-0.15
92	-0.4	0.1	0.0	0.2	17.60	-0.14
93	-0.2	0.2	-0.2	0.3	17.67	1.64
96	-0.7	0.2	-0.6	0.2	17.64	1.68
97	0.3	0.1	0.0	0.3	17.64	-0.10
98	0.1	0.1	0.0	0.2	17.64	1.01
99	0.2	0.2	0.2	0.1	17.65	-0.11
100	-0.2	0.1	-0.1	0.1	17.64	1.53

**Table 7**  
(Continued)

Star ID	$\mu_{\alpha} \cos \delta$ (mas yr <sup>-1</sup> )	$\sigma$ (mas yr <sup>-1</sup> )	$\mu_{\delta}$ (mas yr <sup>-1</sup> )	$\sigma$ (mas yr <sup>-1</sup> )	$R$ (mag)	$(B - R)$ (mag)
102	-0.2	0.1	0.1	0.1	17.66	-0.03
104	0.1	0.2	-0.5	0.2	17.66	-0.20
105	0.3	0.2	0.1	0.3	17.74	0.21
106	0.1	0.2	-0.4	0.2	17.72	1.57
107	-0.6	0.1	-0.5	0.2	17.68	1.60
108	-0.4	0.2	0.3	0.3	17.70	-0.07
109	-0.2	0.2	0.4	0.2	17.72	1.60
110	0.0	0.1	0.2	0.3	17.70	1.72
112	-0.3	0.4	-0.9	0.3	17.71	1.53
113	-0.5	0.2	-0.2	0.2	17.81	1.53
114	0.2	0.1	0.8	0.1	17.76	-0.26
115	0.1	0.1	0.0	0.1	17.81	1.09
117	0.3	0.3	0.6	0.1	17.76	0.93
118	0.3	0.2	0.6	0.2	17.78	1.39
119	-0.1	0.2	0.5	0.2	17.85	1.54
120	0.6	0.2	0.0	0.2	17.81	1.62
121	-0.9	0.2	0.0	0.2	17.79	1.52
122	0.6	0.1	0.5	0.2	17.78	-0.14
123	-0.3	0.1	0.1	0.1	17.81	1.17
124	-0.5	0.2	0.0	0.2	17.82	1.46
125	0.4	0.2	0.3	0.2	17.79	-0.13
126	0.6	0.3	-0.1	0.1	17.89	-0.13
127	0.6	0.2	0.5	0.3	17.89	0.30
128	-0.3	0.2	-0.6	0.2	17.85	-0.20
130	-0.5	0.2	0.8	0.1	17.87	1.53
131	0.1	0.3	-0.6	0.1	17.85	1.61
132	0.4	0.1	-0.1	0.2	17.82	-0.14
133	0.3	0.2	-0.3	0.1	17.84	1.60
134	0.4	0.3	0.2	0.3	17.90	1.14
135	0.4	0.2	-0.3	0.2	17.89	1.52
138	-0.4	0.2	0.1	0.2	17.88	1.32
139	0.1	0.2	0.2	0.2	17.89	-0.04
141	0.2	0.3	0.8	0.2	17.95	-0.17
142	-0.2	0.1	-0.2	0.2	18.01	1.30
143	-0.7	0.2	-0.2	0.3	17.94	-0.12
146	0.0	0.1	0.6	0.3	17.97	1.31
147	-0.3	0.1	0.1	0.2	17.97	1.43
148	-0.3	0.2	0.5	0.2	18.00	-0.07
149	0.4	0.2	-0.2	0.2	18.00	1.50
150	-0.2	0.1	0.6	0.1	18.01	-0.10
152	0.3	0.1	0.3	0.1	18.05	-0.08
153	0.5	0.1	0.9	0.2	18.07	1.29
154	-0.3	0.2	0.3	0.3	18.04	1.45
155	-0.3	0.2	-1.0	0.3	18.04	0.03
156	0.0	0.2	0.3	0.2	18.05	1.00
157	0.1	0.3	0.7	0.2	18.04	1.17
158	0.6	0.2	-0.5	0.3	18.02	1.15
159	-0.2	0.2	-0.7	0.2	18.01	1.15
160	-0.4	0.2	-0.4	0.3	18.08	1.50
161	0.3	0.2	-0.6	0.1	18.06	-0.25
162	0.3	0.2	-0.3	0.2	18.06	1.41
163	0.5	0.3	-0.3	0.1	18.04	-0.26
164	0.7	0.2	0.3	0.2	18.06	-0.10
165	-0.6	0.2	-0.1	0.2	18.10	-0.05
166	-0.3	0.2	0.7	0.3	18.13	-0.05
169	-0.5	0.2	0.1	0.1	18.10	1.55
170	0.4	0.3	-0.3	0.4	18.12	-0.06
171	0.0	0.1	-0.5	0.3	18.15	1.37
172	0.3	0.1	-0.3	0.2	18.07	0.22
173	-0.4	0.2	0.1	0.2	18.12	1.11
175	0.4	0.4	-0.2	0.2	18.14	-0.12
176	0.0	0.2	0.7	0.3	18.12	1.54
177	0.2	0.5	0.4	0.4	18.16	1.24
178	0.7	0.2	0.2	0.2	18.16	1.47
179	-0.3	0.2	-0.7	0.3	18.19	1.47



**Table 7**  
(Continued)

Star ID	$\mu_{\alpha} \cos \delta$ (mas yr <sup>-1</sup> )	$\sigma$ (mas yr <sup>-1</sup> )	$\mu_{\delta}$ (mas yr <sup>-1</sup> )	$\sigma$ (mas yr <sup>-1</sup> )	$R$ (mag)	$(B - R)$ (mag)
182	0.2	0.2	0.1	0.2	18.18	1.48
183	0.6	0.3	0.3	0.4	18.22	1.41
185	0.0	0.2	-0.4	0.2	18.27	-0.13
187	-0.2	0.3	-0.6	0.3	18.21	-0.13
188	0.0	0.2	-0.3	0.2	18.23	1.61
189	-0.1	0.2	0.6	0.2	18.23	-0.17
190	0.2	0.1	-0.7	0.2	18.19	-0.13
191	0.3	0.3	0.5	0.2	18.27	1.58
192	-0.7	0.3	0.4	0.1	18.22	1.16
193	-0.3	0.2	0.2	0.2	18.28	-0.01
196	0.2	0.3	-0.6	0.1	18.23	-0.16
199	-0.1	0.2	-0.6	0.3	18.28	1.15
202	-0.2	0.2	0.4	0.2	18.31	1.15
203	-0.7	0.3	-0.2	0.2	18.27	1.44
204	0.3	0.2	0.1	0.2	18.28	1.32
205	-0.2	0.1	0.0	0.2	18.33	1.35
206	0.2	0.2	0.4	0.2	18.31	1.35
207	-0.3	0.2	0.2	0.2	18.28	-0.09
210	-0.3	0.3	-0.1	0.3	18.32	-0.04
212	0.1	0.3	-0.1	0.3	18.43	1.16
215	0.1	0.1	0.6	0.1	18.35	-0.08
216	0.4	0.4	-0.2	0.2	18.35	-0.14
217	-0.3	0.2	0.2	0.2	18.33	1.64
219	-0.2	0.3	-0.5	0.3	18.31	1.47
222	-0.7	0.2	0.0	0.2	18.39	-0.18
224	0.7	0.3	-0.3	0.2	18.37	1.20
229	0.2	0.3	-0.3	0.2	18.37	-0.08
230	0.1	0.4	0.8	0.3	18.46	1.11
232	0.6	0.2	0.2	0.3	18.39	1.48
233	0.0	0.2	-0.2	0.2	18.36	1.14
234	0.5	0.2	0.8	0.2	18.38	1.34
235	0.0	0.1	0.3	0.2	18.40	-0.13
236	-0.2	0.2	-0.1	0.3	18.40	-0.14
237	0.0	0.2	-0.2	0.2	18.44	1.27
241	0.1	0.2	0.9	0.2	18.42	1.49
242	-0.1	0.2	0.3	0.2	18.39	1.15
243	-0.3	0.3	0.4	0.2	18.46	-0.17
247	-0.4	0.5	0.3	0.3	18.45	0.85
248	0.4	0.3	-0.6	0.6	18.50	1.26
249	0.0	0.2	0.1	0.3	18.47	-0.05
250	0.1	0.2	0.1	0.2	18.46	1.47
251	-0.2	0.1	-0.2	0.2	18.46	-0.11
253	0.2	0.7	-0.2	0.3	18.61	1.28
254	-0.4	0.2	-0.1	0.2	18.43	1.40
255	0.0	0.2	0.5	0.2	18.47	1.08
258	-0.2	0.2	0.4	0.2	18.49	1.24
260	-0.2	0.2	-0.4	0.2	18.49	1.45
261	-0.3	0.3	-0.4	0.2	18.45	-0.15
262	0.2	0.2	0.3	0.2	18.52	1.59
264	-0.5	0.3	0.2	0.2	18.46	1.41
266	-0.5	0.1	-0.4	0.2	18.45	1.41
267	0.0	0.2	0.2	0.3	18.52	1.16
268	0.3	0.3	-0.3	0.2	18.56	1.11
269	-0.3	0.2	-0.5	0.2	18.56	-0.13
270	-0.2	0.1	0.1	0.2	18.48	1.28
271	0.1	0.3	-0.4	0.3	18.66	1.18
272	0.2	0.3	0.2	0.2	18.50	1.17
275	-0.2	0.2	0.2	0.2	18.47	1.31
276	-0.1	0.2	0.8	0.1	18.59	1.43
277	-0.2	0.2	-0.2	0.2	18.56	-0.05
278	0.1	0.4	-0.1	0.2	18.57	1.41
282	0.4	0.1	-0.2	0.2	18.55	1.28
283	0.3	0.3	-0.6	0.2	18.61	1.36
287	-0.6	0.3	0.6	0.3	18.57	1.09
289	-0.2	0.3	-0.2	0.3	18.59	1.23

**Table 7**  
(Continued)

Star ID	$\mu_{\alpha} \cos \delta$ (mas yr <sup>-1</sup> )	$\sigma$ (mas yr <sup>-1</sup> )	$\mu_{\delta}$ (mas yr <sup>-1</sup> )	$\sigma$ (mas yr <sup>-1</sup> )	$R$ (mag)	$(B - R)$ (mag)
292	-0.3	0.2	0.8	0.3	18.69	-0.07
293	0.1	0.1	0.9	0.2	18.59	-0.12
297	0.4	0.2	0.3	0.2	18.62	-0.09
298	0.2	0.2	-0.4	0.2	18.65	-0.04
300	-0.3	0.1	-0.6	0.3	18.67	-0.07
301	0.0	0.4	0.3	0.4	18.69	0.90
302	0.5	0.3	0.2	0.2	18.65	1.23
303	-0.1	0.2	0.2	0.2	18.70	1.24
304	-0.3	0.2	0.0	0.2	18.69	1.42
305	-0.2	0.3	0.3	0.3	18.65	1.48
306	-0.7	0.3	-0.5	0.3	18.70	-0.01
307	-0.5	0.2	0.3	0.2	18.63	-0.16
310	-0.7	0.2	0.1	0.2	18.68	1.26
312	-0.1	0.2	-0.6	0.3	18.72	1.10
313	0.3	0.2	-0.4	0.2	18.68	-0.09
314	0.7	0.2	-0.4	0.4	18.83	0.06
315	0.3	0.3	0.0	0.2	18.73	1.26
316	0.1	0.3	0.7	0.3	18.70	1.15
319	0.1	0.3	0.2	0.3	18.75	1.17
320	-0.2	0.3	0.3	0.3	18.77	-0.07
321	-0.1	0.1	-0.4	0.2	18.70	1.57
322	-0.1	0.1	0.5	0.3	18.72	1.57
323	0.4	0.2	0.1	0.1	18.75	1.24
324	0.3	0.2	-0.8	0.2	18.76	1.28
326	0.2	0.1	-0.1	0.2	18.75	-0.11
328	0.3	0.2	0.1	0.4	18.80	-0.04
329	0.1	0.3	-0.2	0.3	18.80	-0.12
331	0.1	0.2	0.5	0.2	18.72	-0.02
335	0.2	0.2	0.0	0.2	18.78	-0.09
336	0.1	0.2	-0.3	0.3	18.87	1.19
338	-0.4	0.1	0.2	0.2	18.75	1.28
340	-0.8	0.2	0.5	0.2	18.73	1.25
341	0.0	0.1	0.1	0.2	18.69	1.43
342	0.2	0.2	-0.4	0.3	18.85	-0.12
343	-0.5	0.1	-0.4	0.2	18.75	1.24
344	0.7	0.3	-0.6	0.2	18.79	1.22
345	0.0	0.2	0.6	0.2	18.76	1.16
346	-0.8	0.3	0.1	0.3	18.84	-0.05
347	-0.5	0.3	-0.4	0.2	18.76	1.40
348	0.6	0.2	-0.6	0.2	18.80	1.21
349	-0.1	0.2	-0.1	0.3	18.91	0.89
350	-0.1	0.2	0.7	0.2	18.79	1.24
351	0.4	0.2	0.3	0.2	18.89	1.22
354	-0.7	0.2	0.2	0.3	18.89	0.00
355	-0.5	0.2	-0.3	0.2	18.77	-0.12
357	0.5	0.1	-0.3	0.3	18.82	1.13
358	0.1	0.2	0.7	0.3	18.83	1.10
359	0.0	0.2	-0.3	0.2	18.85	1.38

R.A. and 0.413 mas yr<sup>-1</sup> in decl. (QJ0035-7201,  $N_{\text{stars}} = 126$ ), 0.419 mas yr<sup>-1</sup> in R.A. and 0.351 mas yr<sup>-1</sup> in decl. (QJ0047-7530,  $N_{\text{stars}} = 82$ ), 0.397 mas yr<sup>-1</sup> in R.A. and 0.424 mas yr<sup>-1</sup> in decl. (QJ0102-7546,  $N_{\text{stars}} = 98$ ), and 0.373 mas yr<sup>-1</sup> in R.A. and 0.431 mas yr<sup>-1</sup> in decl. (QJ0111-7249,  $N_{\text{stars}} = 243$ ). As it can be seen, these values are comparable to the proper motion uncertainty for our QSOs.

$BR$  photometry in these tables is from Noël et al. (2007), and it was used to construct  $R$  versus  $(B - R)$  CMDs with the purpose of detecting possible dependencies of our results on the color of the reference stars (caused in turn by population-dependent internal motions and/or unknown systematic astrometric effects) and a possible contamination of our SFRs by

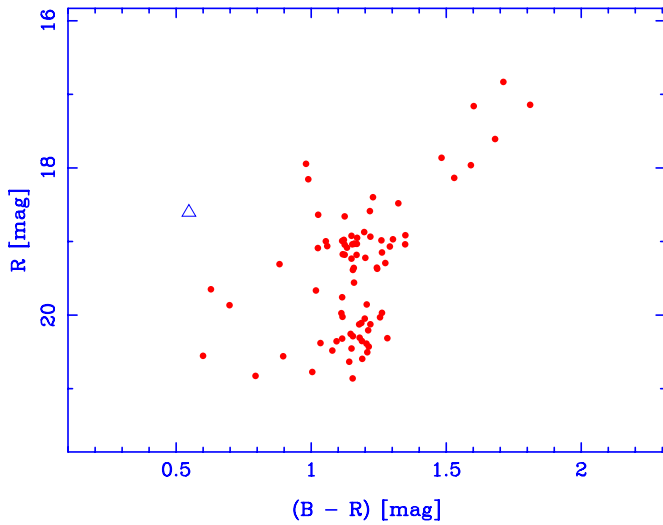


**Figure 11.**  $R$  vs.  $(B - R)$  color-magnitude diagram of the stars used to define the reference frame in the field of QJ0033–7028. The background QSO is indicated by a triangle. This diagram was constructed using calibrated photometry obtained for the SMC fields by Noël et al. (2007), in the course of our study of the star formation history of the SMC. Examination of the present diagram and of that given in the above reference indicates that there is little or no contamination by Galactic foreground stars.  
(A color version of this figure is available in the online journal.)

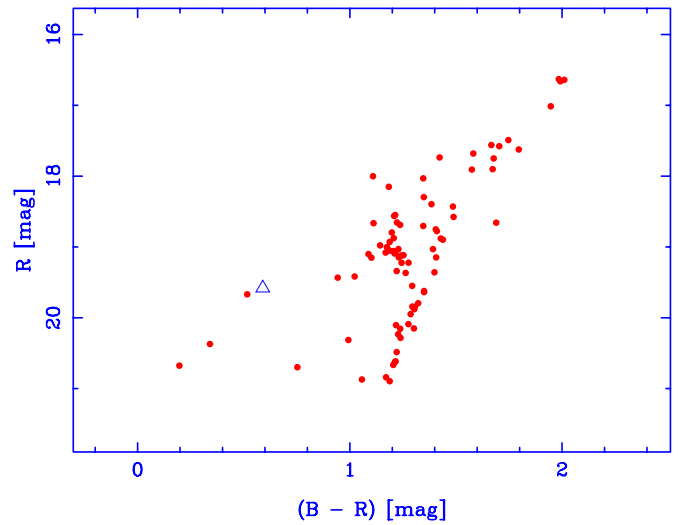


**Figure 13.** Same as Figure 11, for field QJ0047–7530.  
(A color version of this figure is available in the online journal.)

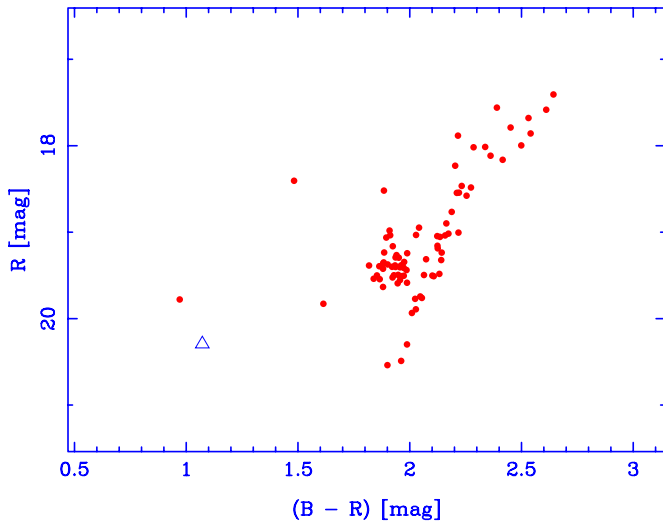


**Figure 12.** Same as Figure 11, for field QJ0035–7201.  
(A color version of this figure is available in the online journal.)

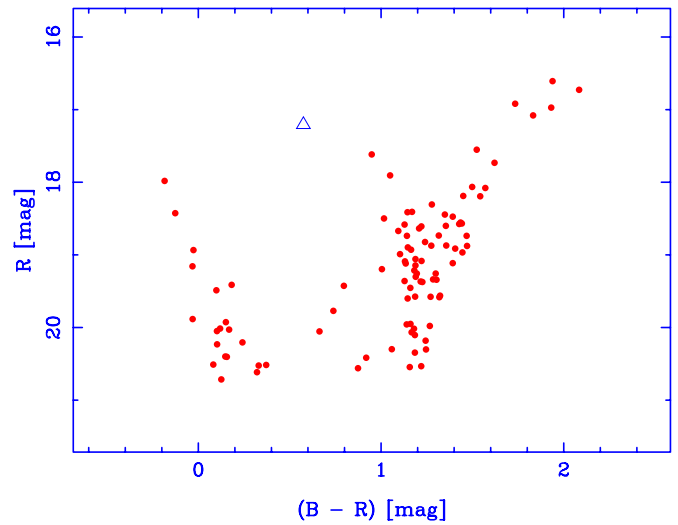


**Figure 14.** Same as Figure 11, for field QJ0102–7546.  
(A color version of this figure is available in the online journal.)

Galactic foreground stars. These CMDs are presented in Figures 11–15.

In the case of fields QJ0033–7028, QJ0035–7201, and QJ0047–7530, the number of blue objects among the reference stars is too small for such tests to be meaningful; nonetheless, we still evaluated the effect of removing the few bluer reference stars seen in Figures 11–13. In all three cases, the exclusion of these stars increased the error of the fit (see the next section), albeit not changing the proper motion significantly (confirming what was reported in CMP09). On the contrary, by having a distinct and fairly numerous population of blue stars, fields QJ0102–7546 and QJ0111–7249 provided a good ground for these tests (the latter field in particular).

In the case of field QJ0111–7249, by dividing the “blue” (79 objects) and “red” (163 objects) populations at  $(B - R)$

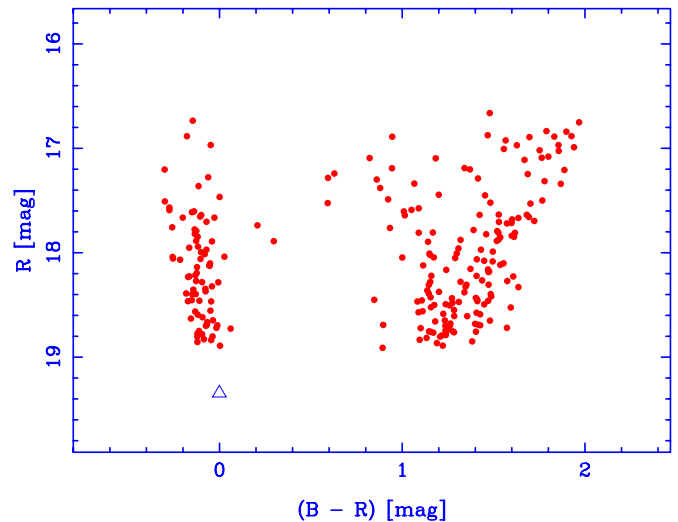


**Figure 15.** Same as Figure 11, for field QJ0111–7249.  
(A color version of this figure is available in the online journal.)

**Table 8**  
Mean Barycentric Positions for QJ0033–7028

Epoch	$\bar{\alpha}_{bc}$ (arcsec)	$\sigma$ (mas)	$\bar{\delta}_{bc}$ (arcsec)	$\sigma$ (mas)	$N$
2001.799	1.557	0.6	-33.656	0.7	6
2002.780	1.553	0.6	-33.658	1.1	7
2003.809	1.553	0.7	-33.657	0.8	6
2004.847	1.551	1.1	-33.655	3.0	3
2005.832	1.550	0.7	-33.651	0.8	9
2006.802	1.556	0.7	-33.650	0.5	10
2007.776	1.548	0.4	-33.649	0.8	10
2008.830	1.550	0.5	-33.650	1.0	6

**Table 9**  
Mean Barycentric Positions for QJ0035–7201

Epoch	$\bar{\alpha}_{bc}$ (arcsec)	$\sigma$ (mas)	$\bar{\delta}_{bc}$ (arcsec)	$\sigma$ (mas)	$N$
2001.800	39.681	1.5	-20.051	3.1	6
2002.782	39.688	2.6	-20.045	1.7	5
2003.809	39.689	0.5	-20.049	1.6	6
2004.847	39.680	3.9	-20.048	3.0	3
2005.835	39.687	0.7	-20.041	0.9	5
2006.804	39.686	1.2	-20.041	1.3	9
2007.776	39.682	2.2	-20.038	1.4	7
2008.834	39.676	1.6	-20.043	1.9	10

$\sim 0.4$  mag, we obtained final proper motions of  $\mu_{\alpha} \cos \delta = +0.11 \pm 0.20$  mas yr $^{-1}$ ,  $\mu_{\delta} = -0.67 \pm 0.19$  mas yr $^{-1}$  (red sample) and  $\mu_{\alpha} \cos \delta = -0.15 \pm 0.26$  mas yr $^{-1}$ ,  $\mu_{\delta} = -0.82 \pm 0.21$  mas yr $^{-1}$  (blue sample), both consistent (better than  $1\sigma$ ) with the result obtained including all stars given in Table 13. In the case of field QJ0102–7546, the division of populations was also made at  $(B - R) \sim 0.4$  mag, and we obtained final proper motions of  $\mu_{\alpha} \cos \delta = +0.94 \pm 0.22$  mas yr $^{-1}$ ,  $\mu_{\delta} = -2.47 \pm 0.16$  mas yr $^{-1}$  (red sample, 78 objects) and  $\mu_{\alpha} \cos \delta = +1.09 \pm 0.32$  mas yr $^{-1}$ ,  $\mu_{\delta} = -1.96 \pm 0.35$  mas yr $^{-1}$  (blue sample, 20 objects), again both consistent with the result obtained including all stars given in Table 13. The larger difference seen in the case of the blue sample is a consequence of the small number and poor distribution of reference stars (as reflected by larger error in the final proper motion). We have therefore used all stars, regardless of their color, in our final SFRs.

The fact that our results are not affected by obvious population-dependent internal motions is a very important clue when interpreting our “as measured” proper motion results (see Section 4) for fields QJ0047–7530, QJ0102–7546, and QJ0111–7249, which seem to be affected by streaming motions.

Examination of Figures 11–13 also indicates that there is little or no contamination by Galactic foreground stars in the corresponding SFRs.

### 3.6. Proper Motions

As is the case of non-SMC stars, the QSO does not conform to the SFR either, so its standard coordinates will also change with time. Because QSOs can be considered fiducial points, this motion with respect to the SFR is no more than the reflection of the motion of the local reference system of SMC stars. This motion is also determined via a linear regression, and the *negative* slope of the straight line adjusted to the standard

**Table 10**  
Mean Barycentric Positions for QJ0047–7530

Epoch	$\bar{\alpha}_{bc}$ (arcsec)	$\sigma$ (mas)	$\bar{\delta}_{bc}$ (arcsec)	$\sigma$ (mas)	$N$
2001.798	19.602	1.5	-30.067	2.1	6
2002.777	19.601	1.6	-30.070	1.0	7
2003.811	19.600	1.9	-30.067	1.1	3
2004.847	19.598	3.1	-30.066	3.6	3
2005.832	19.599	1.2	-30.055	0.4	7
2006.800	19.598	0.8	-30.055	1.2	11
2008.830	19.594	0.9	-30.056	1.8	4

**Table 11**  
Mean Barycentric Positions for QJ0102–7546

Epoch	$\bar{\alpha}_{bc}$ (arcsec)	$\sigma$ (mas)	$\bar{\delta}_{bc}$ (arcsec)	$\sigma$ (mas)	$N$
2001.798	19.734	1.1	-29.911	0.9	6
2002.782	19.736	0.6	-29.909	0.4	7
2003.816	19.734	0.8	-29.911	1.1	6
2004.850	19.730	0.7	-29.906	0.2	3
2005.836	19.731	0.4	-29.905	0.9	8
2006.800	19.737	0.8	-29.899	0.8	9
2007.777	19.729	0.9	-29.896	0.9	12
2008.834	19.727	0.4	-29.897	0.8	9

**Table 12**  
Mean Barycentric Positions for QJ0111–7249

Epoch	$\bar{\alpha}_{bc}$ (arcsec)	$\sigma$ (mas)	$\bar{\delta}_{bc}$ (arcsec)	$\sigma$ (mas)	$N$
2001.797	31.851	1.3	-9.815	0.8	6
2002.781	31.847	1.3	-9.809	0.9	6
2003.815	31.851	1.6	-9.807	0.9	6
2004.848	31.849	1.1	-9.802	1.5	4
2005.833	31.848	0.8	-9.807	0.4	7
2006.804	31.853	0.7	-9.808	0.8	13
2007.778	31.846	0.8	-9.806	0.5	9
2008.833	31.850	0.9	-9.807	0.9	6

coordinates versus epoch diagram for the QSO will then give the proper motion of the corresponding SMC field.

### 3.7. Results

In Tables 8–12, we give the DCR-corrected mean barycentric positions, as a function of epoch, of the background QSOs in fields QJ0033–7028, QJ0035–7201, QJ0047–7530, QJ0102–7546, and QJ0111–7249, respectively; together with their standard deviations and the number of points used to calculate the mean for each epoch.

In Figures 16–20, we present the corresponding barycentric position versus epoch diagrams. The values of R.A. and decl. in these figures are the individual positions of the QSOs on different frames relative to the barycenter (bc) of the SFR. The lines plotted are the best-fit lines resulting from a linear regression analysis on the data, with all points having the same weight. The negative values of their slopes correspond to the actual proper motion of the barycenter of the reference stars.

In Table 13, we present the “as measured” field proper motions obtained for the five QSO fields reported in this paper. As explained in Section 3.5, the errors assigned to these proper motions were computed as the formal error of the slope in



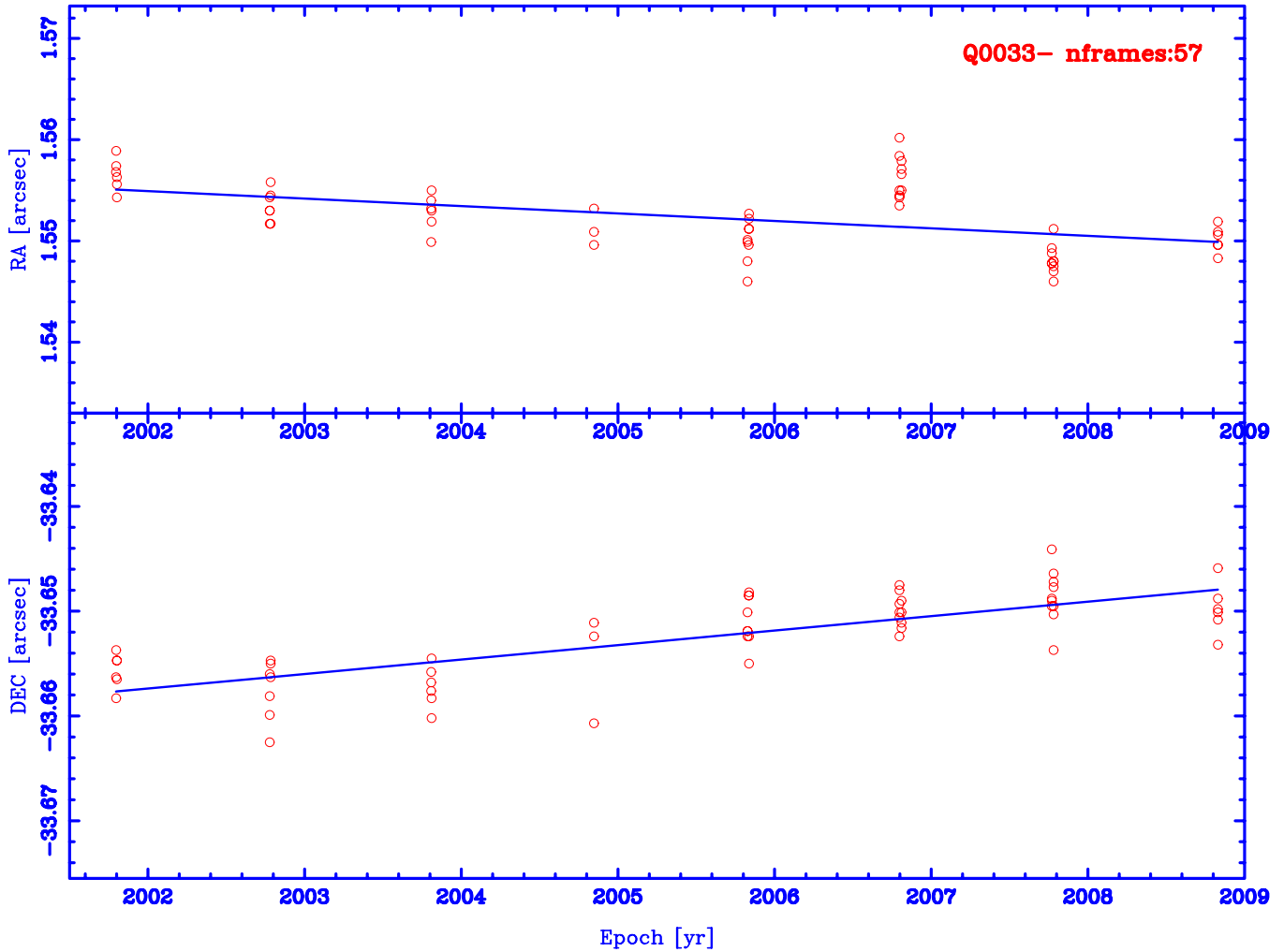


**Figure 16.** Barycentric position vs. epoch diagram for QJ0033–7028. The values of R.A. and decl. are the individual positions of the QSO on different frames relative to the barycenter (bc) of the SFR. The lines shown are the best-fit lines resulting from a linear regression analysis on the data. The *negative* values of their slopes correspond to the actual proper motion of the barycenter of the SMC reference stars:  $\mu_{\alpha} \cos \delta = +0.73 \pm 0.18 \text{ mas yr}^{-1}$  and  $\mu_{\delta} = -1.38 \pm 0.16 \text{ mas yr}^{-1}$ . See Tables 8 and 13.

(A color version of this figure is available in the online journal.)

**Table 13**  
As Measured Field Proper Motions

SMC Field	$\mu_{\alpha} \cos(\delta)$ (mas yr <sup>-1</sup> )	$\mu_{\delta}$ (mas yr <sup>-1</sup> )
QJ0033–7028	$+0.73 \pm 0.18$	$-1.38 \pm 0.16$
QJ0035–7201	$+0.91 \pm 0.33$	$-1.39 \pm 0.31$
QJ0047–7530	$+0.97 \pm 0.23$	$-2.55 \pm 0.33$
QJ0102–7546	$+0.94 \pm 0.19$	$-2.39 \pm 0.16$
QJ0111–7249	$+0.06 \pm 0.21$	$-0.71 \pm 0.19$

the straight-line fit, and thus include *all* sources of positional uncertainty.

### 3.8. CCD Orientation

The proper motions derived above are in the approximate (R.A., decl.) directions given by the orientation of the corresponding SFR, which does not necessarily coincide with the Equatorial System for a given Equinox. To evaluate/correct for this possible effect, we have to find the orientation of the SFRs with respect to the International Celestial Reference frame (ICRF; Arias et al. 1995), which is done by comparison with the

Guide Star Catalog, version 2.2 (GSC2.2, 2001).<sup>6</sup> To accomplish this we used the IRAF tasks CCXYMATCH and CCMAP instead of the procedure described in CMP09, the major difference being that in the present procedure we only used stars included in our SFRs to determine the orientations, while in the former method *all* GSC2.2 stars found in our images were used.

Our SFRs were found to have a negligible rotation with respect to the ICRF, namely,  $-0^{\circ}.76 \pm 0^{\circ}.012$  (QJ0033–7028),  $+0^{\circ}.26 \pm 0^{\circ}.011$  (QJ0035–7201),  $+0^{\circ}.22 \pm 0^{\circ}.013$  (QJ0047–7530),  $-0^{\circ}.44 \pm 0^{\circ}.003$  (QJ0102–7546), and  $-0^{\circ}.42 \pm 0^{\circ}.011$  (QJ0111–7249).

As a natural outcome of the procedure, a mean plate scale was obtained in each case:  $0.2601 \pm 0^{\circ}.000015 \text{ pixel}^{-1}$  (QJ0033–7028),  $0.2605 \pm 0^{\circ}.000039 \text{ pixel}^{-1}$  (QJ0035–7201),  $0.2604 \pm 0^{\circ}.000073 \text{ pixel}^{-1}$  (QJ0047–7530),  $0.2605 \pm 0^{\circ}.000028 \text{ pixel}^{-1}$  (QJ0102–7546), and  $0.2605 \pm 0^{\circ}.000009 \text{ pixel}^{-1}$  (QJ0111–7249).

With this new method, for field QJ0036–7227 presented in CMP09, we now find a rotation of  $-0^{\circ}.75 \pm 0^{\circ}.007$  and obtain

<sup>6</sup> Space Telescope Science Institute, 2001, The Guide Star Catalog, version 2.2.01.

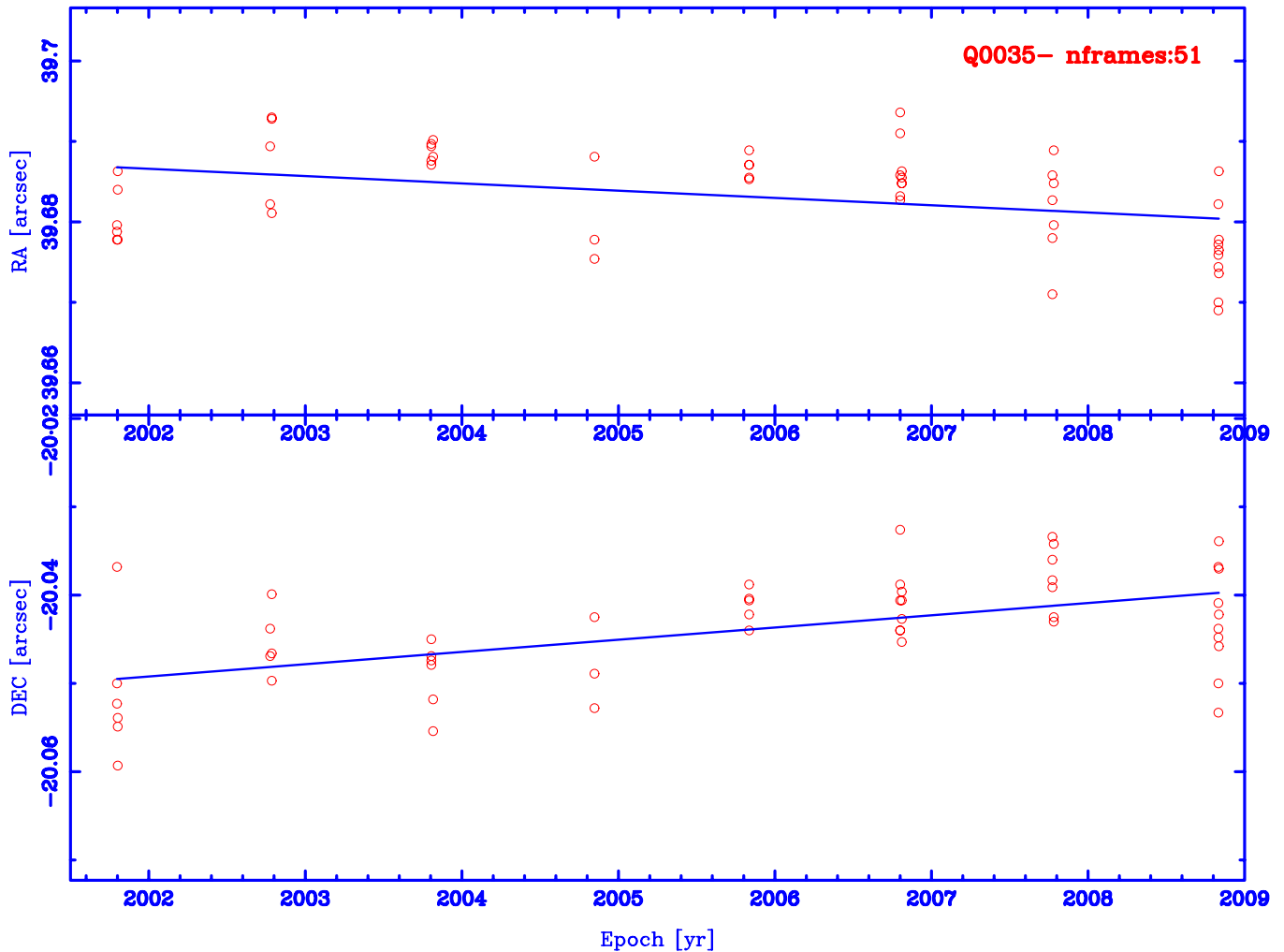


**Figure 17.** Same as Figure 16, for field QJ0035–7201.  $\mu_{\alpha} \cos \delta = +0.91 \pm 0.33 \text{ mas yr}^{-1}$  and  $\mu_{\delta} = -1.39 \pm 0.31 \text{ mas yr}^{-1}$ . See Tables 9 and 13. (A color version of this figure is available in the online journal.)

a plate scale of  $0.2605 \pm 0'.000005 \text{ pixel}^{-1}$ . The much smaller errors achieved here, in comparison to those given in CMP09, can be explained by the nature of the procedure used in CMP09, which allows for objects with contaminated PSFs to be included in the solution.

These values differ only  $\sim 1\%$  from the nominal plate scale ( $0'.259 \text{ pixel}^{-1}$ ), so we used this latter throughout our study.

#### 4. CENTER-OF-MASS PROPER MOTIONS

For details we refer the reader to Section 4 of CMP09.

The proper motion results presented in Table 13 are “as measured” (field) values. If we want to derive the motion of the CM of the SMC, we have to remove (possible) perspective and rotation effects from our measured proper motions. The former is a purely geometric projection effect due to the angular separation in the sky between our fields and the corresponding CM, and the latter is due to internal systemic motions.

To accomplish this we have applied the method presented by Jones et al. (1994, hereafter JKL94). In CMP09, we discuss why we have not used the newer, more sophisticated, procedure proposed by van der Marel et al. (2002, hereafter vDM02). In the JKL94 procedure it is assumed that all field (reference) stars are at the same distance, in the principal plane of a disk, and that there is no contamination from a kinematical halo. Required

input parameters are the equatorial coordinates of the field of interest (defined by the coordinates of the background QSO) and of the center of the SMC, the heliocentric distance of the center of the SMC, the inclination of the galaxy’s disk and position angle of the line of the nodes, and the rotational and the radial velocity at the position of the field of interest.

There is no clear evidence of rotation in the case of the SMC (see Harris & Zaritsky 2006, hereafter HZ06; Piatek et al. 2008, hereafter PI08), so a rotation correction to our SMC field proper motions is not needed. On the other hand, our QSO fields lie at angular distances ranging from  $\sim 1.4$  to  $\sim 3.3$  from the main body of the SMC, so a perspective correction is still necessary. We must note at this point that, for reasons that will be explained in Section 4.2 (Discussion), we will present CM proper motions only for fields QJ0033–7028 and QJ0035–7201.

To realize the latter via the JKL94 procedure, we must assume that the SMC has a disklike central structure and that our QSO fields lie in the principal plane of this component. The existence of a disklike structure is supported by the results of Stanimirović et al. (2004), based on a study of the distribution and kinematics of HI in the SMC, but it must be kept in mind that it is possible that the distribution and kinematics of the gaseous and stellar components may be different. We note, for example, that, based on a study of red giants, HZ06 conclude that the SMC is primarily supported by its velocity dispersion.

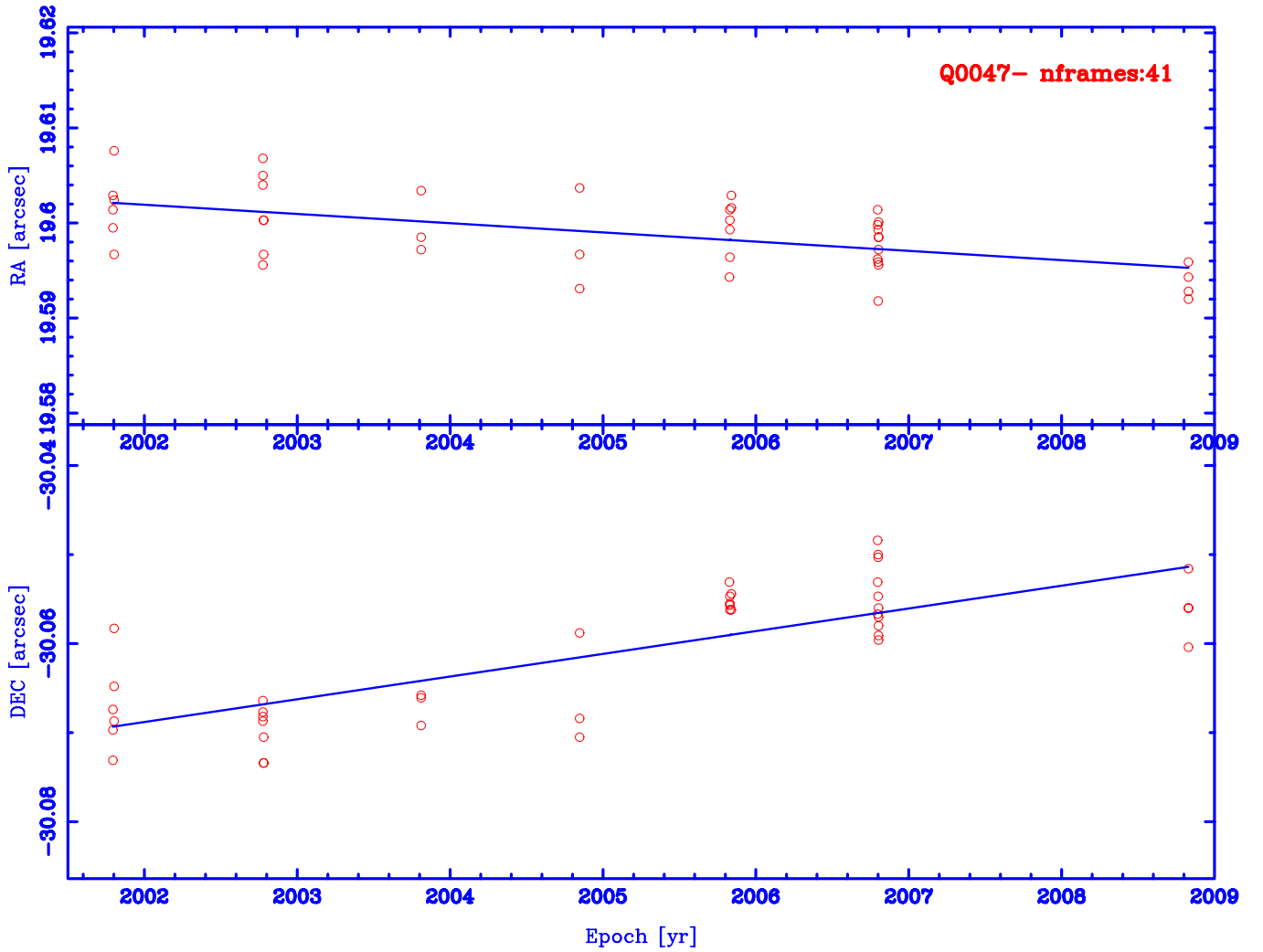


**Figure 18.** Same as Figure 16, for field QJ0047–7530.  $\mu_{\alpha} \cos \delta = +0.97 \pm 0.23$  mas yr $^{-1}$  and  $\mu_{\delta} = -2.55 \pm 0.33$  mas yr $^{-1}$ . See Tables 10 and 13. (A color version of this figure is available in the online journal.)

We have adopted the following values for the required input parameters.

Field coordinates (R.A., decl.):

QJ0033–7028: (8:48, –70:48) J2000.0, from Tinney (1999).

QJ0035–7201: (8:87, –72:02) J2000.0, from Tinney et al. (1997).

SMC center coordinates: (R.A., decl.) = (13:20, –72:50) J2000.0; kinematical center, from PI08.

Heliocentric distance of the SMC center: 61.7 kpc, corresponding to a distance modulus of  $m - M = 18.95$ , from Cioni et al. (2000).

Inclination of the disk: ( $i = 40^\circ$ ), from Stanimirović et al. (2004).

Position angle (P.A.) of the descending node of the lines of nodes: ( $40^\circ$ ), also from Stanimirović et al. (2004).

Although measured radial velocities are available for our SMC fields (Carrera 2006; Carrera et al. 2008), for consistency with the JKL94 method we will not use the Carrera results and apply the procedure as if in the absence of measured velocities. In the JKL94 methodology, it is required that the radial velocity of a given field must be such that the derived radial velocity for the CM of the galaxy corresponds to standard values for this quantity.

**Table 14**  
Center-of-mass Proper Motions

SMC Field	$\mu_{\alpha} \cos(\delta)$ (mas yr $^{-1}$ )	$\mu_{\delta}$ (mas yr $^{-1}$ )
QJ0033–7028	$+0.86 \pm 0.19$	$-1.34 \pm 0.15$
QJ0035–7201	$+1.02 \pm 0.33$	$-1.34 \pm 0.29$

To recover the currently accepted radial velocity for the CM of the SMC ( $+146.0 \pm 0.6$  km s $^{-1}$ ; HZ06) via the JKL94 prescription, it is necessary to adopt  $+125.6$  km s $^{-1}$  and  $+136.1$  km s $^{-1}$  as the radial velocities of fields QJ0033–7028 and QJ0035–7201, respectively. Interestingly, Carrera (2006) and Carrera et al. (2008) obtain mean radial velocities at the position of our fields of  $+131$  km s $^{-1}$ , with a dispersion of  $39$  km s $^{-1}$  (QJ0033–7028), and  $+153$  km s $^{-1}$ , with a dispersion of  $26$  km s $^{-1}$  (QJ0035–7201). It should be noted, however, that the stars targeted by Carrera in these fields are not exactly the same as we used to define our reference systems in these fields.

In Table 14, we present the resulting CM proper motions for fields QJ0033–7028 and QJ0035–7201 after applying the perspective corrections.



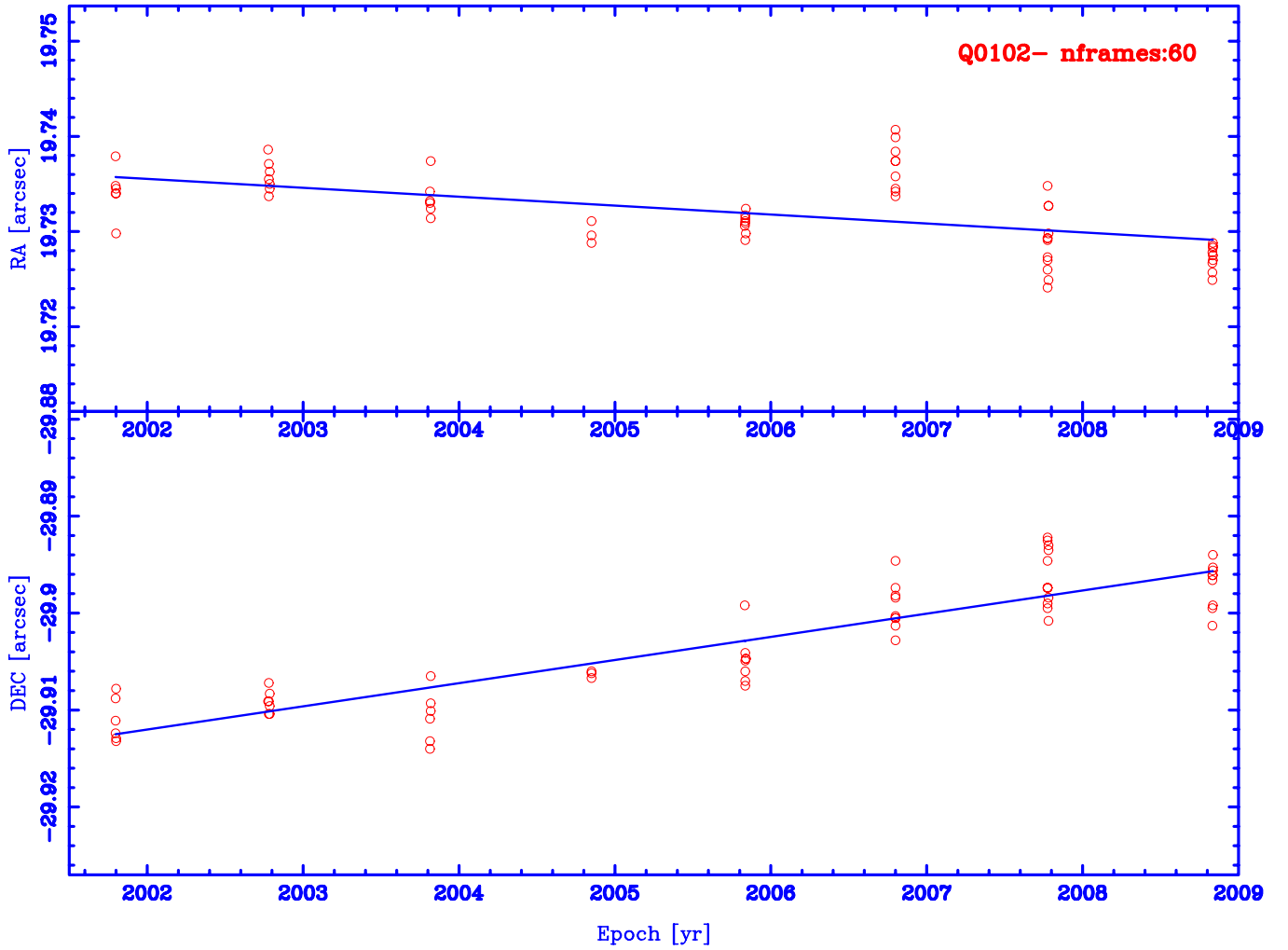


**Figure 19.** Same as Figure 16, for field QJ0102–7546.  $\mu_{\alpha} \cos \delta = +0.94 \pm 0.19 \text{ mas yr}^{-1}$  and  $\mu_{\delta} = -2.39 \pm 0.16 \text{ mas yr}^{-1}$ . See Tables 11 and 13. (A color version of this figure is available in the online journal.)

**Table 15**  
Proper Motion Determinations for the SMC

Source	$\mu_{\alpha} \cos(\delta)$ (mas yr <sup>-1</sup> )	$\mu_{\delta}$ (mas yr <sup>-1</sup> )	Proper Motion System
Kroupa et al. 1994 (F)	$+0.5 \pm 1.0$	$-2.0 \pm 1.4$	PPM Catalog
Kroupa & Bastian 1997 (F)	$+1.23 \pm 0.84$	$-1.21 \pm 0.75$	<i>Hipparcos</i> Catalog
K06a (F) <sup>a</sup>	$+1.16 \pm 0.18$	$-1.17 \pm 0.18$	QSO
PI08 (CM) <sup>b</sup>	$+0.754 \pm 0.061$	$-1.252 \pm 0.058$	QSO
VGA10 (CM)	$+0.98 \pm 0.30$	$-1.10 \pm 0.29$	SPM Catalog
CMP09 (F) <sup>c</sup>	$+0.95 \pm 0.29$	$-1.14 \pm 0.18$	QSO
CMP09 (CM) <sup>c</sup>	$+1.03 \pm 0.29$	$-1.09 \pm 0.18$	QSO
This work (F) <sup>d</sup>	$+0.81 \pm 0.14$	$-1.23 \pm 0.11$	QSO
This work (CM) <sup>d</sup>	$+0.93 \pm 0.14$	$-1.25 \pm 0.11$	QSO

**Notes.** (F) As measured field proper motion. (CM) Center-of-mass proper motion.

<sup>a</sup> Weighted mean of five QSO fields.

<sup>b</sup> Weighted mean of five QSO fields.

<sup>c</sup> From QSO field Q0036–7227.

<sup>d</sup> Weighted mean of three QSO fields: Q0033–7028, Q0035–7201, and Q0036–7227 (CMP09).

#### 4.1. Comparison with Other Proper Motion Results

In Table 15, we summarize our results together with some of the latest results for the proper motion of the SMC available in the literature. (F) stands for field proper motions, while (CM) stands for center-of-mass proper motions. CMP09 stands for our

result for field QJ0036–7227. The numbers presented in “This work” are weighted means, which include the proper motion presented in CMP09.

Examination of this table shows that our result (weighted mean) is in good agreement with recent investigations of the proper motion of the SMC, in particular with the *Hubble Space*

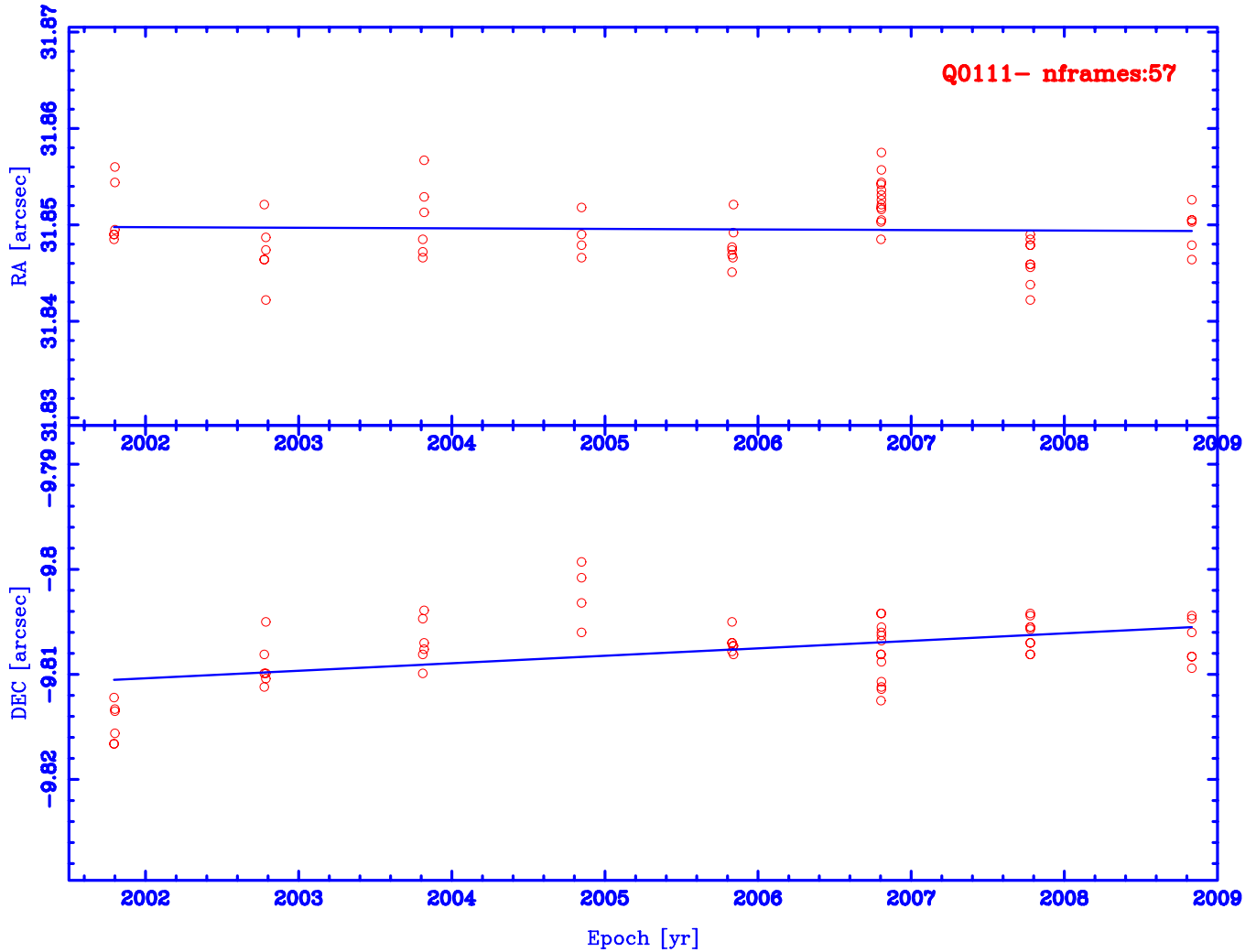


**Figure 20.** Same as Figure 16, for field QJ0111–7249.  $\mu_{\alpha} \cos \delta = +0.06 \pm 0.21 \text{ mas yr}^{-1}$  and  $\mu_{\delta} = -0.71 \pm 0.19 \text{ mas yr}^{-1}$ . See Tables 12 and 13. (A color version of this figure is available in the online journal.)

*Telescope (HST)* result by PI08 and also the result by Vieira et al. (2010, hereafter VGA10). We note that the SMC proper motion from VGA10, presented in Table 15, is their direct determination given in *their* Table 3. This clarification is needed because VGA10 also present a more precise determination of the SMC’s proper motion, combining their relative SMC/LMC motion with more precise LMC proper motions from the literature.

We consider that a more detailed analysis based on the data presented in this table is not appropriate. Proper motion values from different fields cannot be compared directly because they are affected by different perspective and rotation effects. On the other hand, CM proper motions are obtained via an elaborated procedure in which various assumptions are made, and, to further complicate comparisons, all results may additionally be affected by *unidentified* systematic errors. We believe nonetheless that our mean CM proper motion, as well as those derived by *HST* and VGA10, are good representations of the “bulk” transverse motion of the SMC.

#### 4.2. Discussion

As mentioned before, we are confident that the mean CM SMC proper motion listed in Table 15, based on fields QJ0033–7028, QJ0035–7201, and QJ0036–7227, is a good representation of the “bulk” transverse motion of the SMC. A

quick look at Figure 2 of CMP09 shows that these three fields are located to the northwest, west, and west, respectively, of the main body of the SMC.

On the contrary, the “as measured” results we have obtained for fields QJ0047–7530, QJ0102–7546, and QJ0111–7249, located to the south, south, and east of the main body of the SMC, respectively, seem to be affected by streaming motions and were not considered adequate to derive CM proper motions. These streaming motions could be the first direct kinematical evidence (via transverse motions) that the SMC was tidally disrupted in a close encounter with the LMC.

The idea that the SMC was tidally disrupted by the LMC is fairly old and probably originated from the morphological appearance of its eastern side, which is oriented toward the LMC (see, e.g., Ardeberg & Maurice 1978; Irwin et al. 1996), and on theoretical grounds (see, e.g., Murai & Fujimoto 1980; Kroupa et al. 1994; Gardiner & Noguchi 1996). More recently, it has been supported by the studies of the kinematics of its carbon stars (see, e.g., Kunkel et al. 2000), but until now there has been no clear kinematical evidence, via transverse motions, to support this paradigm. We believe that this is most probably due to the fact that, with the exception of our absolute SMC proper motion survey, other *precise* surveys (e.g., *HST*) have relied *only* on fields close to its main body. The VGA10 survey

**Table 16**  
SMC Proper Motion and Space Velocity Components,  
from Field Q0033–7028

Parameter	Value
$\mu_\alpha \cos \delta$ , Field (mas yr <sup>-1</sup> )	0.73 ± 0.18
$\mu_\delta$ , Field (mas yr <sup>-1</sup> )	-1.38 ± 0.16
$\mu_\alpha \cos \delta$ , CM (mas yr <sup>-1</sup> )	0.86 ± 0.19
$\mu_\delta$ , CM (mas yr <sup>-1</sup> )	-1.34 ± 0.15
$\mu_\alpha^{\text{grf}} \cos \delta$ (mas yr <sup>-1</sup> )	0.4 ± 0.1
$\mu_\delta^{\text{grf}}$ (mas yr <sup>-1</sup> )	-0.9 ± 0.1
$\mu_l^{\text{grf}} \cos b$ (mas yr <sup>-1</sup> )	-0.4 ± 0.1
$\mu_b^{\text{grf}}$ (mas yr <sup>-1</sup> )	0.9 ± 0.1
$\Pi$ , velocity component (km s <sup>-1</sup> )	-6 ± 38
$\Theta$ , velocity component (km s <sup>-1</sup> )	-230 ± 35
$Z$ , velocity component (km s <sup>-1</sup> )	185 ± 33
$V_{\text{gc,r}}$ , radial velocity (km s <sup>-1</sup> )	10 ± 32
$V_{\text{gc,t}}$ , transverse velocity (km s <sup>-1</sup> )	295 ± 33

**Table 17**  
SMC Proper Motion and Space Velocity Components,  
from Field Q0035–7201

Parameter	Value
$\mu_\alpha \cos \delta$ , Field (mas yr <sup>-1</sup> )	0.91 ± 0.33
$\mu_\delta$ , Field (mas yr <sup>-1</sup> )	-1.39 ± 0.31
$\mu_\alpha \cos \delta$ , CM (mas yr <sup>-1</sup> )	1.02 ± 0.33
$\mu_\delta$ , CM (mas yr <sup>-1</sup> )	-1.34 ± 0.29
$\mu_\alpha^{\text{grf}} \cos \delta$ (mas yr <sup>-1</sup> )	0.6 ± 0.3
$\mu_\delta^{\text{grf}}$ (mas yr <sup>-1</sup> )	-0.9 ± 0.2
$\mu_l^{\text{grf}} \cos b$ (mas yr <sup>-1</sup> )	-0.6 ± 0.3
$\mu_b^{\text{grf}}$ (mas yr <sup>-1</sup> )	0.9 ± 0.2
$\Pi$ , velocity component (km s <sup>-1</sup> )	31 ± 70
$\Theta$ , velocity component (km s <sup>-1</sup> )	-254 ± 65
$Z$ , velocity component (km s <sup>-1</sup> )	185 ± 61
$V_{\text{gc,r}}$ , radial velocity (km s <sup>-1</sup> )	15 ± 59
$V_{\text{gc,t}}$ , transverse velocity (km s <sup>-1</sup> )	316 ± 63

does cover an extensive area of the SMC, but, possibly because of its design, it could not detect these streaming motions.

It is very important to note that fields QJ0047–7530 and QJ0102–7546, both located to the south of the main body, give almost identical “as measured” proper motions. Given that they come from *completely independent data sets*, of equal quality, we are confident about their reality. Field QJ0111–7249 (also based on excellent data) yields a completely different “as measured” proper motion that could also be explained by streaming motions. This latter field is located to the east of the main body, a region of the SMC that has always been considered likely to have chaotic motion, as suggested by its morphology (Irwin et al. 1996).

Despite the confidence we have in the quality of our data, given the far-reaching implications of our results, we plan to secure a final epoch for these three problematic fields. This will increase the number of epochs to 11 and the time base to 10 years, which should put our results in an unquestionable basis. In this last epoch we will also conclude our observations of two other eastern fields targeted by this survey (QJ0112–7236 and QJ0116–7529), whose preliminary results (albeit with less data) also appear to be in conflict.

## 5. GALACTOCENTRIC SPATIAL VELOCITIES

We ultimately want to determine the space velocities of the SMC with respect to the center of our galaxy, knowledge of which can be used to determine its orbit, and therefore the history of interactions with the LMC and the MW. To accomplish this, we have to project our CM proper motion into the Galactic ( $\mu_l, \mu_b$ ) system, and then calculate the velocity components in the Galactic ( $u, v, w$ ) system. To calculate all spatial velocities and rotation corrections, we used an ad hoc code developed by one of the authors (M.H.P.). This program yields results consistent with an independent software developed by S. Piatek (2005, private communication). A detailed description of the procedure can be found in CMP09.

We note again that, for the reasons explained in Section 4.2 (Discussion), we will present space velocity components only for fields QJ0033–7028 and QJ0035–7201.

From the CM proper motion of the SMC derived from the fields QJ0033–7028 and QJ0035–7201 (presented in Table 14), we obtain

$$\begin{aligned} \text{QJ0033–7028:} \\ V_{\text{gc,r}} = +10 \pm 32 \text{ km s}^{-1}, \end{aligned}$$

**Table 18**  
Galactocentric Velocity Components of the SMC

Source	$V_{\text{gc,r}}$ (km s <sup>-1</sup> )	$V_{\text{gc,t}}$ (km s <sup>-1</sup> )
Kroupa & Bastian 1997	+9 ± 177	+226 ± 177
K06a	+23 ± 7	+301 ± 52
PI08	+6.8 ± 2.4	+259 ± 17
CMP09; from field Q0036–7227	+20 ± 44	+258 ± 50
This work; from field Q0033–7028	+10 ± 32	+295 ± 33
This work; from field Q0035–7201	+15 ± 59	+316 ± 63
This work <sup>a</sup>	+14 ± 24	+289 ± 25

**Note.** <sup>a</sup> Weighted mean of three QSO fields: Q0033–7028, Q0035–7201, and Q0036–7227 (CMP09).

$$\begin{aligned} V_{\text{gc,t}} = +295 \pm 33 \text{ km s}^{-1}, \\ \text{QJ0035–7201:} \end{aligned}$$

$$\begin{aligned} V_{\text{gc,r}} = +15 \pm 59 \text{ km s}^{-1}, \\ V_{\text{gc,t}} = +316 \pm 63 \text{ km s}^{-1}, \end{aligned}$$

where  $V_{\text{gc,r}}$  and  $V_{\text{gc,t}}$  are the galactocentric radial velocity and tangential velocity components of the SMC, respectively.

Tables 16 and 17 summarize all of the proper motion and velocity information obtained for these two fields throughout our procedure. Rows 1 and 2 give field proper motion components and rows 3 and 4 give the corresponding CM proper motion components, both in equatorial coordinates. Rows 5–8 give the corresponding proper motions relative to the Galactic Rest Frame in equatorial and galactic coordinates (see Equation (7), CMP09). Rows 9–11 give the  $\Pi$ ,  $\Theta$ , and  $Z$  components of the galactocentric velocities and rows 12 and 13 the radial and tangential galactocentric velocities, respectively.

In Table 18, we compare our galactocentric radial and tangential velocities for the SMC with published results. There, we present our individual results for fields QJ0033–7028, QJ0035–7201, and QJ0036–7272 (this latter from CMP09) and also a weighted mean based on these three fields. Within the declared uncertainties, there is a good agreement with previous results.

### 5.1. Relative Velocity of the Magellanic Clouds

The relative velocity between the LMC and the SMC can be derived from their  $\Pi$ ,  $\Theta$ , and  $Z$  components, given in Tables 11, 12, and 13 of CMP09 and in Tables 16 and 17 of this paper. We note that although there is a “typo” in Table 13 of

**Table 19**  
Relative Velocity between the LMC and the SMC

Source	$V_{\text{rel}}(\text{LMC/SMC})$ ( $\text{km s}^{-1}$ )
K06a	$105 \pm 42$
PI08	$142 \pm 19$
CMP09 ( $V_{\text{rot,LMC}} 50 \text{ km s}^{-1}$ )	$84 \pm 50$
CMP09 ( $V_{\text{rot,LMC}} 120 \text{ km s}^{-1}$ )	$62 \pm 63$
VGA10	$89 \pm 54$
This work <sup>a</sup> ( $V_{\text{rot,LMC}} 50 \text{ km s}^{-1}$ )	$67 \pm 42$
This work <sup>a</sup> ( $V_{\text{rot,LMC}} 120 \text{ km s}^{-1}$ )	$98 \pm 48$

**Note.** <sup>a</sup> SMC  $\Pi$ ,  $\Theta$ , and  $Z$  velocity components determined from the weighted mean of three QSO fields: Q0033–7028, Q0035–7201, and Q0036–7227 (CMP09).

CMP09 (the sign of  $\Pi$  for the SMC is incorrect), the calculations made in CMP09 used the proper value.

The weighted means of  $\Pi$ ,  $\Theta$ , and  $Z$  for our three SMC fields are  $19 \pm 29$ ,  $-229 \pm 26$ , and  $170 \pm 25$ , respectively, and we recall that in CMP09, we presented two sets of its  $\Pi$ ,  $\Theta$ , and  $Z$  velocity components for the LMC. They correspond to two extreme values of its maximum (constant) rotational velocity (the maximum velocity was adopted because of the large distance of our only LMC QSO field from the LMC center):  $V_{\text{rot,LMC}} 50 \text{ km s}^{-1}$  (obtained from the radial velocities of carbon stars, which is closer to the more widely accepted value of  $50\text{--}60 \text{ km s}^{-1}$ ) and  $120 \text{ km s}^{-1}$  (derived by PI08, from the gradient of their measured proper motions).

For the former value we obtain  $V_{\text{rel}}(\text{LMC/SMC}) = 67 \pm 42 \text{ km s}^{-1}$  and for the latter  $V_{\text{rel}}(\text{LMC/SMC}) = 98 \pm 48 \text{ km s}^{-1}$ . Our high internal errors prevent strong conclusions about the gravitational binding of the MCs, but to illustrate we note that simple point-mass models indicate that for  $M_{\text{LMC}} \sim 2 \times 10^{10} M_{\odot}$  (Schommer et al. 1992), the escape velocity of the SMC from the LMC is  $\sim 90 \text{ km s}^{-1}$  ( $2 \times 10^{10} M_{\odot}$  is a conservative value adopted in most numerical studies; see, e.g., Gardiner & Noguchi 1996). In this oversimplified scenario, and albeit our large errors, our relative velocities are consistent with the standard assumption that the MCs are gravitationally bound to each other.

In Table 19, we summarize recent determinations of the relative velocity between the LMC and SMC. A quick look at this table shows that, given that  $V_{\text{rel}}(\text{LMC/SMC})$  is very sensitive to the errors of the proper motions, the dilemma of the binarity of the MCs is far from being settled. We note that models by K06a, based on the theoretical platform originally developed by Murai & Fujimoto (1980), but using the data presented in Kallivayalil et al. (2006b) and Kallivayalil et al. (2006a, hereafter K06a), are consistent with both bound and unbound orbits.

## 6. CONCLUSIONS

Here we summarize the main conclusions of this work.

1. We present new results from a program to determine the proper motions of the MCs using QSOs in their background as reference points, namely, for fields QJ0033–7028, QJ0035–7201, QJ0047–7530, QJ0102–7546, and QJ0111–7249 of the SMC.
2. The “as measured” field proper motions obtained for fields QJ0033–7028 and QJ0035–7201, located, respectively, to the northwest and west of the main body of SMC, are in good agreement with the result published in CMP09 for

field QJ0036–7227 (located to the west of the main body of the SMC) and also with *HST* results (K06b and PI08) from fields located near the main body of the SMC.

3. Assuming that the SMC has a disklike central structure and that it does not rotate, applying a perspective correction to the above three field proper motions leads to a CM proper motion (weighted mean of fields QJ0033–7028, QJ0035–7201, and QJ0036–7227) for the SMC of  $\mu_{\alpha} \cos \delta = +0.93 \pm 0.14 \text{ mas yr}^{-1}$ ,  $\mu_{\delta} = -1.25 \pm 0.11 \text{ mas yr}^{-1}$ , in good agreement with recent results by PI08 and VGA10.
4. We are confident that the result from the above three fields from our survey is a good representation of the “bulk” transverse motion of the SMC (as is the case of the fields targeted by *HST* on the main body of the SMC). This is not the case of the results we have obtained for fields QJ0047–7530, QJ0102–7546, and QJ0111–7249, which seem to be affected by streaming motions. It is for this reason that we have not derived CM proper motions using the field proper motions determined for the latter.
5. Fields QJ0047–7530 and QJ0102–7546, both located to the south of the main body of the SMC, give almost identical “as measured” proper motions. We stress that the field proper motions obtained for these two fields come from *completely independent data sets* of equal quality, which gives us confidence about their reality. Field QJ0111–7249 also yields a conflictive “as measured” proper motion, that could also be explained by streaming motions. This latter field is located to the east of the main body of the SMC, a region that has always been considered likely to have chaotic motion, as suggested by its morphology.
6. Complementing our proper motion data for the SMC with the currently accepted radial velocity of its center ( $+146.0 \text{ km s}^{-1}$ ; HZ06), we have derived its galactocentric (gc) velocity components. Combining the result given in CMP09 with those presented here, we obtain (weighted mean)  $V_{\text{gc,t}} = +289 \pm 25 \text{ km s}^{-1}$  and  $V_{\text{gc,r}} = +14 \pm 24 \text{ km s}^{-1}$ .
7. These velocities, together with the galactocentric velocity components given for the LMC in CMP09, imply a relative velocity between the LMC and SMC of  $67 \pm 42 \text{ km s}^{-1}$  for  $V_{\text{rot,LMC}} = 50 \text{ km s}^{-1}$  and of  $98 \pm 48 \text{ km s}^{-1}$  for  $V_{\text{rot,LMC}} = 120 \text{ km s}^{-1}$ . Albeit our large errors, these values are consistent with the standard assumption that the MCs are gravitationally bound to each other.

E.C. and R.A.M. acknowledge support by the Fondo Nacional de Investigación Científica y Tecnológica (proyectos Fondecyt No. 1050718 y No. 1070312), the Chilean Centro de Astrofísica (FONDAP No. 15010003), and the Chilean Centro de Excelencia en Astrofísica y Tecnologías Afines (PFB 06). M.H.P. acknowledges support by the Fondo Nacional de Investigación Científica y Tecnológica (proyecto No. 1050718 Fondecyt) and by the Universidad de Tarapacá research fund (project # 4721-09). M.M. acknowledges support by the Fondo Nacional de Investigación Científica y Tecnológica (proyecto No. 1050718 Fondecyt). C.G. and N.N. acknowledge support by the Instituto de Astrofísica de Canarias (P3-94) and by the Ministry of Education and Research of the Kingdom of Spain (AYA2004-06343).

## REFERENCES

Ardeberg, A., & Maurice, E. 1978, *Acad. Sci. Paris C. R. Ser. B Sci. Phys.*, **286**, 375



- Arias, E. F., Charlot, P., Feissel, M., & Lestrade, J.-F. 1995, *A&A*, **303**, 604
- Bevington, P. R. 1969, *Data Reduction and Error Analysis for the Physical Sciences* (New York: McGraw-Hill)
- Carrera, R. 2006, PhD thesis, Universidad de la Laguna, Tenerife, Spain
- Carrera, R., Gallart, C., Aparicio, A., Costa, E., Méndez, R. A., & Noël, N. E. D. 2008, *AJ*, **136**, 1039
- Cioni, M.-R. L., van der Marel, R. P., Loup, C., & Habing, H. J. 2000, *A&A*, **359**, 601
- Costa, E., Méndez, R. A., Pedreros, M. H., Moyano, M., Gallart, C., Noël, N., Baume, G., & Carraro, G. 2009, *AJ*, **137**, 4339
- Gardiner, L. T., & Noguchi, M. 1996, *MNRAS*, **278**, 191
- Harris, J., & Zaritsky, D. 2006, *AJ*, **131**, 2514
- Irwin, M. J., Demers, S., & Kunkel, W. E. 1996, *BAAS*, **28**, 932
- Jones, B. F., Klemola, A. R., & Lin, D. N. C. 1994, *AJ*, **107**, 1333 (JKL94)
- Kallivayalil, N., van der Marel, R. P., & Alcock, C. 2006a, *ApJ*, **652**, 1213 (K06a)
- Kallivayalil, N., van der Marel, R. P., Alcock, C., Axelrod, T., Cook, K. H., Drake, A. J., & Geha, M. 2006b, *ApJ*, **638**, 772
- Kroupa, P., & Bastian, U. 1997, *New Astron.*, **2**, 77
- Kroupa, P., Röser, S., & Bastian, U. 1994, *MNRAS*, **266**, 412
- Kunkel, W. E., Demers, S., & Irwin, M. J. 2000, *AJ*, **119**, 2789
- Méndez, R. A., Costa, E., Pedreros, M. H., Moyano, M., Altmann, M., & Gallart, C. 2010, *PASP*, **122**, 853
- Murai, T., & Fujimoto, M. 1980, *PASJ*, **32**, 581
- Noël, N. E. D., Aparicio, A., Gallart, C., Hidalgo, S. L., Costa, E., & Méndez, R. A. 2009, *ApJ*, **705**, 1260
- Noël, N. E. D., Gallart, C., Costa, E., & Méndez, R. A. 2007, *AJ*, **133**, 2037
- Piatek, S., Pryor, C., & Olszewski, E. W. 2008, *AJ*, **135**, 1024 (PI08)
- Schommer, R. A., Suntzeff, N. B., Olszewski, E. W., & Harris, H. C. 1992, *AJ*, **103**, 447
- Stanimirović, S., Staveley-Smith, L., & Jones, P. A. 2004, *ApJ*, **604**, 176
- Stetson, P. B. 1987, *PASP*, **99**, 191
- Tinney, C. G. 1999, *MNRAS*, **303**, 565
- Tinney, C. G., Da Costa, G. S., & Zinnecker, H. 1997, *MNRAS*, **285**, 111
- van der Marel, R. P., Alves, D. R., Hardy, E., & Suntzeff, N. B. 2002, *AJ*, **124**, 2639 (vDM02)
- Vieira, K., et al. 2010, *AJ*, **140**, 1934